Journal of Chromatography A 1693 (2023) 463878

Contents lists available at ScienceDirect

Journal of Chromatography A

journal homepage: www.elsevier.com/locate/chroma

Isotherm model discrimination for multimodal chromatography using mechanistic models derived from high-throughput batch isotherm data

Scott H. Altern[a], John P. Welsh[b], Jessica Y. Lyall[c], Andrew J. Kocot[a], Sean Burgess[c], Vijesh Kumar[d], Chris Williams[c], Abraham M. Lenhoff[d], Steven M. Cramer[a,*]

[a] Department of Chemical and Biological Engineering, Rensselaer Polytechnic Institute, Troy, NY, USA
[b] Biologics Process Research and Development, Merck & Co., Inc., Rahway, NJ, USA
[c] Purification Development, Genentech, South San Francisco, CA, USA
[d] Department of Chemical and Biomolecular Engineering, University of Delaware, Newark, DE, USA

ARTICLE INFO

Article history:
Received 25 December 2022
Revised 5 February 2023
Accepted 15 February 2023
Available online 17 February 2023

Keywords:
Multimodal chromatography
Mechanistic modeling
Adsorption isotherm
Model selection
High-throughput experimentation

ABSTRACT

In this work, we have examined an array of isotherm formalisms and characterized them based on their relative complexities and predictive abilities with multimodal chromatography. The set of isotherm models studied were all based on the stoichiometric displacement framework, with considerations for electrostatic interactions, hydrophobic interactions, and thermodynamic activities. Isotherm parameters for each model were first determined through twenty repeated fits to a set of mAb – Capto MMC batch isotherm data spanning a range of loading, ionic strength, and pH as well as a set of mAb – Capto Adhere batch data at constant pH. The batch isotherm data were used in two ways—spanning the full range of loading or consisting of only the high concentration data points. Predictive ability was defined through the model's capacity to capture prominent changes in salt gradient elution behavior with respect to pH for Capto MMC or unique elution patterns and yield losses with respect to gradient slope for Capto Adhere. In both cases, model performance was quantified using a scoring metric based on agreement in peak characteristics for column predictions and accuracy of fit for the batch data. These scores were evaluated for all twenty isotherm fits and their corresponding column predictions, thereby producing a statistical distribution of model performances. Model complexity (number of isotherm parameters) was then considered through use of the Akaike information criterion (AIC) calculated from the score distributions. While model performance for Capto MMC benefitted substantially from removal of low protein concentration data, this was not the case for Capto Adhere; this difference was likely due to the qualitatively different shapes of the isotherms between the two resins. Surprisingly, the top-performing (high accuracy with minimal number of parameters) isotherm model was the same for both resins. The extended steric mass action (SMA) isotherm (containing both protein-salt and protein-protein activity terms) accurately captured both the pH-dependent elution behavior for Capto MMC as well as loss in protein recovery with increasing gradient slope for Capto Adhere. In addition, this isotherm model achieved the highest median score in both resin systems, despite it lacking any explicit hydrophobic stoichiometric terms. The more complex isotherm models, which explicitly accounted for both electrostatic and hydrophobic interaction stoichiometries, were ill-suited for Capto MMC and had lower AIC model likelihoods for Capto Adhere due to their increased complexity. Interestingly, the ability of the extended SMA isotherm to predict the Capto Adhere results was largely due to the protein-salt activity coefficient, as determined via isotherm parameter sensitivity analyses. Further, parametric studies on this parameter demonstrated that it had a major impact on both binding affinity and elution behavior, therein fully capturing the impact of hydrophobic interactions. In summary, we were able to determine the isotherm formalisms most capable of consistently predicting a wide range of column behavior for both a multimodal cation-exchange and multimodal anion-exchange resin with high accuracy, while containing a minimized set of model parameters.

* Corresponding author.
E-mail address: crames@rpi.edu (S.M. Cramer).

https://doi.org/10.1016/j.chroma.2023.463878
0021-9673/

1. Introduction

Multimodal chromatographic systems have been demonstrated to exhibit distinct selectivity [1–4] compared to single-mode systems—ion-exchange chromatography (IEC) and hydrophobic interaction chromatography (HIC)—resulting in its utility in tackling complex protein purification challenges [5–7]. This selectivity is driven by the synergistic combination of multiple interaction types (e.g., electrostatic and hydrophobic) [8,9]. Electrostatic repulsion is expected to decrease the binding affinity with increasing salt concentration, while hydrophobic interaction is expected to increase binding affinity (i.e., retention) [10,11]. The relationship of affinity with salt concentration can be qualitatively different between multimodal cation-exchange (MMCEX) and multimodal anion-exchange (MMAEX) resins. More specifically, MMCEX typically exhibits monotonic (strictly decreasing) affinity with respect to ionic strength [12], but can develop a U-shape pattern at very high salt concentrations ($\sim$ 2 M NaCl) and low pH (near the pKa of the resin) [13]. In contrast, MMAEX can see the transition to a hydrophobically-dominated regime at much lower salt concentrations at pHs near the isoelectric point (pI) of the protein [14,15]. At pHs below the pI, increased electrostatic repulsion reduces binding strength at low ionic strength; however, at high ionic strength, increased hydrophobic interactions can again promote binding [16]. It is worth noting that these two scenarios for MMAEX are akin to those seen in hydrophobic interaction chromatography (HIC) [17,18].

While U-shaped retention trends have been shown to exist in MMAEX systems, the impact that they have on column elution behavior under nonlinear adsorption conditions has not been well-characterized [19]. Fortunately, elution behavior under U-shaped binding conditions in HIC have been characterized by Creasy et al. [20,21] for lysozyme and two mAbs with elution using ammonium sulfate. These studies illustrated that the U-shaped trend in binding affinity is associated with elution recovery losses. Importantly, recovery was shown to be dependent on gradient slope which led to the definition of a critical gradient slope—where additional increases in slope further decrease recovery. This phenomenon arises from the salt gradient moving too quickly in reference to the velocity of the protein, resulting in desorption and subsequent adsorption (re-binding) of the protein along the column axial coordinate. In other words, the protein must “see” the salt concentration of the U-shape minima long enough (according to the chromatographic velocity of the protein) to complete elution and maximize recovery. While this finding has not yet been shown for multimodal resins, it is plausible that similar behavior could occur.

Despite this gap in the understanding of multimodal systems, investigations have identified crucial considerations for practical use of multimodal ligands, which may increase the difficulty of process development [22,23]. These include the presence of broad elution peaks and associated losses in protein recovery [19,24–26] caused by the inordinate impact of hydrophobic interactions. Certain advantages of multimodal systems can even lead to problematic scenarios. For instance, the prominent pH sensitivity of multimodal provides a valuable handle for tuning its performance [27–29] but also can decrease process robustness if deviations in pH occur (e.g., improper buffer preparation). Naturally, it is critical to understand these behaviors and to employ methods that can shed light on them. To this end, column modeling has been shown to be a useful tool for imparting process understanding [30,31].

In the space of protein chromatography modeling, ion-exchange chromatography (IEC) is arguably the most well-studied [32]. Most efforts in this space have been directed towards prediction of protein elution behavior, which is critical for preparative applications. The adsorption isotherm is at the heart of understanding protein elution and has thus been the focus of most column modeling efforts. There are a variety of adsorption isotherms that can be used to predict protein elution with the most common being the steric mass action (SMA) isotherm [33].

While the SMA isotherm has been used extensively for modeling CEX, it has also been applied successfully for modeling of multimodal cation-exchange (MMCEX) [26,34,35] and multimodal anion-exchange (MMAEX) [19,36,37]. This application is in apparent contrast to the nature of multimodal interactions, which involve both charged and hydrophobic components. Taking a more first-principles-based approach would lead one to think that an isotherm formalism describing both types of interactions would be more appropriate for modeling multimodal chromatography. To this end, isotherm formalisms of increased complexity have been used to model MMCEX [35,38,39] and multimodal anion-exchange (MMAEX) behavior [30]. Two noteworthy isotherm models are those developed by Nfor et al. [12] and Lee et al. [16]. Both isotherm models included stoichiometric terms for electrostatic and hydrophobic interactions as well as thermodynamic activities for protein-protein interactions and protein-salt interactions. The model from Lee et al. [16] also included a stoichiometric term for water displaced during hydrophobic interactions. Nfor et al. [12] showed that batch isotherm data for MMAEX resins and various model proteins containing U-shaped trends could be fit effectively. Column simulations for a small set of the proteins and MMAEX resins studied were also performed [30], however these were limited to very low column loadings where the elution profiles were well-behaved. Lee et al. [16] successfully applied it to predicting mAb retention with U-shape trends in isocratic experiments performed at a range of pH conditions. This application was also limited to the linear adsorption regime and thus did not characterize the mechanistic model’s ability to predict elution behavior under nonlinear loading conditions. While some mechanistic models have been developed for multimodal chromatographic systems, their application has been mostly limited to prediction of column behavior under linear adsorption conditions. Further, no studies (to the best of the authors’ knowledge) have demonstrated that the complex elution behavior, under nonlinear adsorption conditions, in multimodal systems—stemming from isotherms with U-shaped affinity vs. ionic strength trends—have been predicted with a mechanistic isotherm model.

It is important to note that while these isotherm formalisms better describe the interactions present in multimodal systems compared to SMA, their complexity results in them having many parameters which can make them more cumbersome to employ. More specifically, having larger sets of model parameters is tied to challenges in parameter identifiability, namely the ability to reliably determine parameter values [40,41]. For example, parameter values obtained from fitting a complex model to experimental data may vary substantially without influencing the quality of the fit [42]. This issue can become obvious when applying the model towards extrapolated conditions where poorly-determined model parameters may produce inaccurate predictions [43]. Further, the computational expense of parameter estimation increases with the number of parameters which can be particularly problematic for expensive objective functions such as those required for inverse fitting of chromatographic profiles [44]. Overall, it is preferable to employ models of reduced complexity that can achieve the same level of predictive accuracy as more complex models.

Recent work has been done to deploy simplified models for multimodal chromatography. Importantly, Hess et al. [45] illustrated that the electrostatic terms in the isotherm construction can be effectively ignored when the system (MMAEX, in this case) at pHs far below the protein isoelectric point, contains minimal contributions from electrostatic interactions. In this regime, the relationship of binding affinity with respect to salt concentration is expected to be monotonically increasing; as such, it is reasonable to

assume a functional form that only considers hydrophobic interactions. Hahn et al. [46] also focused on MMAEX, however the focus was centered around modeling of pH-based elution instead of salt. Here, the colloidal particle adsorption (CPA) model [47,48] was extended with the asymmetric activity coefficient from Mollerup's thermodynamic framework [49–52], specifically with the protein-salt activity term. This model, while not containing any stoichiometric hydrophobic terms, was able to capture the elution behavior for a MMAEX resin with respect to a wide range of pH conditions and a narrow range of salt conditions for high protein loadings. However, this investigation did not identify if their model would capture elution behavior under a broad range of salt conditions where U-shape binding trends may be present.

This study aims to address the question: is it necessary to use complex isotherm models that account for the full scope of interactions in multimodal chromatography, or can simpler models reasonably be employed? We addressed this with a rigorous analysis of isotherm model performance for formalisms of varying complexity. Model parameters for several isotherm formalisms were determined from fitting batch data for both the MMCEX resin Capto MMC and the MMAEX resin Capto Adhere performed at a range of mobile phase conditions and protein loadings. These isotherm models were then used in concert with the general rate model to predict column elution behavior in salt gradients at several pHs for Capto MMC, where the effect of pH on elution peak characteristics was substantial. Additionally, these isotherm formalisms were employed to predict unique elution behavior for Capto Adhere, where losses in protein recovery increased with respect to increasing gradient slope. The abilities of these models to fit the batch data and to predict the column profiles were then compared both visually (agreement with experimental data) and quantitatively (assessment of a novel score metric). Lastly, the impact of model complexity was investigated through assessment of prediction robustness, information criteria, sensitivity analyses, and parametric studies.

2. Theory

2.1. General rate model of chromatography

The general rate model (GRM) [32,53,54] has been widely employed in column modeling and is briefly summarized here. It contains two differential balances that, overall, capture the change in concentration of protein over time t moving along the column, with column (interstitial) porosity ε_e, at distance x and into the resin particle, with bead (intraparticle) porosity ε_p, at position r. Eq. (1) describes the fluid phase (interstitial) concentration c_i of protein i with interstitial velocity u_{int}, axial dispersion D_{ax}, and rate of mass transfer to the resin surface $k_{film,i}$.

$$\frac{\partial c_i}{\partial t} = -u_{int}\frac{\partial c_i}{\partial x} + D_{ax}\frac{\partial^2 c_i}{\partial x^2} - \frac{1-\varepsilon_e}{\varepsilon_e}\frac{3}{r_p}k_{film,i}\left[c_i - c_{p,i}(x,t,r_p)\right] \quad \text{for } t \geq 0 \text{ and } x \in [0,L] \tag{1}$$

Eq. (2) describes the fluid phase concentration $c_{p,i}$ of protein i in the pore volume and solid phase (adsorbed) concentration q_i with effective pore diffusivity $D_{p,i}$.

$$\frac{\partial c_{p,i}}{\partial t} = D_{p,i}\left(\frac{\partial^2 c_{p,i}}{\partial r^2} + \frac{2}{r}\frac{\partial c_{p,i}}{\partial r}\right) - \frac{1-\varepsilon_p}{\varepsilon_p}\frac{\partial q_i}{\partial t} \quad \text{for } t \geq 0,\ x \in [0,L],\ \text{and } r \in [0,r_p] \tag{2}$$

Further, the GRM contains a transient q_i term to characterize the adsorption and desorption process via the adsorption isotherm model. Specifics on the adsorption isotherm formalism are discussed in Section 2.2. The model is completed by applying the Danckwerts boundary conditions Eqs. (3) and (4)

$$\frac{\partial c_i}{\partial x}(0,t) = \frac{u_{int}}{D_{ax}}[c_i(0,t) - c_{in,i}(t)] \text{for } t \geq 0 \tag{3}$$

$$\frac{\partial c_i}{\partial x}(L,t) = 0 \text{ for } t \geq 0 \tag{4}$$

at the column inlet and outlet, respectively, to Eq. (1) and the radial boundary conditions Eqs. (5) and (6)

$$k_{film,i}\left[c_i - c_{p,i}(x,t,r_p)\right] = \varepsilon_p D_{p,i}\frac{\partial c_{p,i}}{\partial r}(x,t,r_p) \quad \text{for } t \geq 0 \text{ and } x \in [0,L] \tag{5}$$

$$\frac{\partial c_{p,i}}{\partial r}(x,t,0) = 0 \text{ for } t \geq 0 \text{ and } x \in [0,L] \tag{6}$$

to Eq. (2). These account for mass conservation at the resin surface and for symmetry at its center, respectively.

2.2. Adsorption isotherm models

The ion-exchange mechanism from which the steric mass action (SMA) [33] isotherm is constructed is shown in Eq. (7),

$$P + \nu SL^{\pm} \rightleftharpoons PL_{\nu}^{\pm} + \nu S \tag{7}$$

where a protein P displaces ν salt counterions S to form the protein-ligand complex $PL_{\nu}^{\pm}$. The SMA isotherm in its kinetic form is shown in Eq. (8),

$$k_{kin,i}\frac{\partial q_i}{\partial t} = K_{eq,i}\left[\Lambda - \sum_{j=1}^{k}\left(\nu_j + \sigma_j\right)q_j\right]^{\nu_i} c_{p,i} - c_s^{\nu_i} q_i \tag{8}$$

where $k_{kin,i}$ is a kinetic rate constant (inverse of the desorption rate) as described by Huuk et al. [55,56], $K_{eq,i}$ is the equilibrium constant for protein component i, ν_i is its characteristic charge (number of stoichiometric charged binding sites), $c_{p,i}$ is its concentration, and c_s is the concentration of the salt counterion. Further, Λ is the ionic capacity of the resin and σ is the steric factor (σ_i referring to the i^{th} kinetic equation and σ_j referring to the j^{th} protein in each equation) representing the average number of shielded counterions, at charged binding sites, by an adsorbed protein molecule. Multicomponent effects are included here by explicitly accounting for each protein component j, out of all protein components k, that compete for the available binding sites. The SMA model can be extended to include an empirical pH dependence [57], where $K_{eq,i}$ is assumed to be an exponential function of pH in Eq. (9)

$$K_{eq,i} = K_{eq0,i}\exp\left[K_{eq1,i}\left(\text{pH} - \text{pH}_{ref}\right)\right] \tag{9}$$

and ν_i is assumed to be a linear function of pH in Eq. (10).

$$\nu_i = \nu_{0,i} + \nu_{1,i}\left(\text{pH} - \text{pH}_{ref}\right) \tag{10}$$

Here, a reference pH pH_{ref} is provided to allow for scaling of the pH-dependent isotherm parameters for convenience. While these functional forms are empirical in nature, it is worth noting that they have some physical basis due to the pH-dependent changes in protein surface charge, due to titration. It is also worth mentioning that these pH-dependencies have been applied successfully in modeling of ion-exchange systems [57–60]. In addition to the pH modification, the SMA model can be further extended by applying the asymmetric activity coefficient from Mollerup's thermodynamic framework [49–52] to obtain the generalized ion-exchange (GIEX) isotherm [61], referred to as the SMA Extended (Ext.) isotherm in this work. This model, in its kinetic form, is shown in Eq. (11),

$$k_{kin,i}\frac{\partial q_i}{\partial t} = K_{eq,i}\tilde{\gamma}_i\left[\Lambda - \sum_{j=1}^{k}\left(\nu_j + \sigma_j\right)q_j\right]^{\nu_i} c_{p,i} - c_s^{\nu_i} q_i \tag{11}$$

where the thermodynamic activity terms $K_{s,i}$ (protein-salt interaction) and $K_{p,i}$ (protein-protein interaction) for protein i are introduced through a modified activity coefficient $\tilde{\gamma}_i$ in Eq. (12).

$$\tilde{\gamma}_i = \frac{\gamma_i}{\gamma^{\infty,\omega}} \approx \exp\left(K_{p,i}c_{p,i} + K_{s,i}c_s\right) \tag{12}$$

Here, $\gamma_i^{\infty,\omega}$ is the activity coefficient of the protein in water at infinite dilution and is assumed to be unity. The remaining parameters here are identical to those in the unmodified SMA model. Another model, called SMA K_s, has the same form as SMA Ext., however the K_p parameter is unused (set to zero). It worth noting that while $K_{s,i}$ and $K_{p,i}$ are also pH-dependent [52], explicit inclusion of pH in its formulation was avoided in order to avoid redundancy with the pH-dependent $K_{eq,i}$ term.

In consideration of the mixed-mode exchange reaction Eq. (13)

$$P + \nu SL^{\pm} + nL \;\rightleftharpoons\; PL_{\nu}^{\pm}L_n + \nu S \tag{13}$$

protein P displaces ν salt counterions S while simultaneously interacting with n hydrophobic ligands to form the protein-ligand complex $PL_{\nu}^{\pm}L_n$. Further, the kinetic form of the isotherm representing this exchange is shown in Eq. (14),

$$k_{kin,i}\frac{\partial q_i}{\partial t} = K_{eq,i}\tilde{\gamma}_i\left[\Lambda - \sum_{j=1}^{k}\left(\nu_j + \sigma_j\right)q_j\right]^{\nu_i} \times\left[\Lambda - \sum_{j=1}^{k}\left(n_j + s_j\right)q_j\right]^{n_i} c_{p,i} - c_s^{\nu_i}q_i \tag{14}$$

which is identical to the isotherm derived by Nfor et al. [12]. This model is similar to the SMA model in its functional form, although with added components to account for the stoichiometry of hydrophobic interactions n_i (analogous to ν_i) and the steric shielding parameter of hydrophobic interactions s (s_i referring to the i^{th} kinetic equation and s_j referring to the j^{th} protein in each equation) which is analogous to σ. This isotherm formalism will be referred to as the Ottens isotherm for the remainder of this work, with a thermodynamic extension analogous to the SMA Ext. model, dubbed Ottens Ext. With respect to the model's pH dependence, a similar extension can be applied with the addition of n_i also being a linear function of pH in Eq. (15).

$$n_i = n_{0,i} + n_{1,i}\left(\mathrm{pH} - \mathrm{pH}_{ref}\right) \tag{15}$$

It is worth noting here that the ionic capacities of charged and hydrophobic sites (Λ^{IEC} and Λ^{HIC}, respectively) are assumed to be identical ($\Lambda^{IEC} = \Lambda^{HIC}$) , which is a reasonable assumption [12,46] if the resin chemistry has a 1:1 ratio of charged to hydrophobic groups. This assumption implies that if $\nu_i = n_i$ and $\sigma_i = s_i$, the saturation capacity for electrostatic interactions $q_{max,i}^{IEC}$ and the saturation capacity for hydrophobic interactions $q_{max,i}^{HIC}$ must be equal to one another (i.e., $q_{\mathrm{max},i}^{IEC} = \Lambda^{IEC}/[\nu_i + \sigma_i] = \Lambda^{HIC}/[n_i + s_i] = q_{\mathrm{max},i}^{HIC}$). However, when these isotherm parameters are not equal, different saturation capacities arise between the two modes. As outlined by Hahn et al. [46], this challenges the assumption of simultaneous binding and, therein, suggests that true saturation capacity is some combination of $q_{max,i}^{IEC}$ and $q_{max,i}^{IEC}$.

Another isotherm that can be used for modeling of multimodal chromatography is the SMA/HIC hybrid isotherm. This isotherm can be obtained by conjoining the hydrophobic interaction chromatography (HIC) isotherm presented by Wang et al. [62] with the SMA Ext. isotherm, in a similar manner as shown for the Ottens isotherm, and is similar to the model presented by Lee et al. [16]. The main difference between the SMA/HIC model and the Ottens model is the addition of the β term, which refers to the stoichiometric number of bulk-like water molecules W that are released to form the protein-ligand complex $PL_{\nu}^{\pm}L_n$ with respect to the hydrophobic component of the multimodal interaction Eq. (16).

$$P + \nu SL^{\pm} + nLW_{\beta} \;\rightleftharpoons\; PL_{\nu}^{\pm}L_n + \nu S + n\beta W \tag{16}$$

From here, the corresponding isotherm formalism, presented in its kinetic form, is shown in Eq. (17).

$$k_{kin,i}\frac{\partial q_i}{\partial t} = K_{eq,i}\tilde{\gamma}_i\left[\Lambda - \sum_{j=1}^{k}\left(\nu_j + \sigma_j\right)q_j\right]^{\nu_i} \times\left[\Lambda - \sum_{j=1}^{k}\left(n_j + s_j\right)q_j\right]^{n_i} c_{p,i} - c_s^{\nu_i}\, q_i^{1+n_i\beta_i} \tag{17}$$

The β_i term is determined by the value of $\beta_{0,i}$ and its exponential salt dependence, scaled with $\beta_{1,i}$ [62] in Eq. (18).

$$\beta_i = \beta_{0,i}\exp\left(\beta_{1,i}c_s\right) \tag{18}$$

With respect to the extensions to this model, the same pH and thermodynamic extensions that were used for the Ottens isotherm formalism can be applied for the SMA/HIC model. Accordingly, the SMA/HIC variant containing the modified activity coefficient will be referred to as the SMA/HIC Ext. isotherm. All these models can be represented in the equilibrium form, used to fit batch data, by setting the left-hand side of the equation to zero. The kinetic forms of these models, as shown, are useful for column simulations where they can be directly applied to the GRM. Importantly, these forms all include the rate constant $k_{kin,i}$, which cannot be obtained from fitting batch data at equilibrium and was thus set to unity for all of the models in this investigation. Lastly, derivations for these isotherm models are provided in SI.1 (Word document).

3. Material and methods

3.1. Materials

Sodium chloride, sodium acetate trihydrate, acetic acid, tris base, tris hydrochloride, sodium hydroxide, hydrochloric acid, sodium azide, and 10 kDa centrifugal filter units were purchased from MilliporeSigma (St. Louis, MO). MAb A (protein A eluate), with an isoelectric point of 8.7, was generously donated by Genentech (South San Francisco, CA). MAb B (protein A eluate), with an isoelectric point of 8.0, was generously donated by Merck & Co., Inc. (Rahway, NJ). Pre-packed OPUS® 1 ml (0.5 cm x 5 cm) MiniChrom Capto MMC and Capto Adhere columns were graciously provided by Repligen (Waltham, MA). HiPrep 26/10 desalting columns were purchased from Cytiva (Malborough, MA). 0.2 μm bottle top vacuum filters, 0.2 μm PES syringe filters, and Luerlock syringes (10 ml and 30 ml) were purchased from VWR (Randor, PA).

3.2. Chemicals and buffers

Buffers for the Capto MMC column experiments were prepared using 20 mM sodium acetate (equilibration buffer) with or without 1.5 M NaCl (elution buffer) at pH 5.3, 5.5, 5.6, 5.9, and 6.2 containing 0.02% (w/w) sodium azide (preservative). Buffers for the Capto Adhere column experiments were prepared using 55 mM tris (equilibration buffer) with or without 1 M NaOAc (elution buffer) at pH 8 containing 0.02% (w/w) sodium azide (preservative). Adjustments on buffer pH were performed, if necessary, with the addition of 6 M NaOH or 6 M HCl until the exact pH was obtained. Buffers for the batch experiments were prepared in an equivalent manner, except different pHs for Capto MMC (5, 5.25, 5.5, and 6). All buffers were 0.2 μm filtered following their preparation.

3.3. mAb sample preparation

Buffer exchange of the mAb A for the Capto MMC batch experiments was performed using 10 kDa centrifugal filter units at 4000 rpm until completion. mAb B was prepared for the Capto Adhere batch experiments by diluting it with buffer stocks to reach the desired fluid composition. Buffer exchange of the mAb A for the Capto MMC column experiments was performed using a Cytiva HiPrep desalting column into pH 5.5 acetate buffer (20 mM) containing 75 mM NaCl. mAb B was exchanged into pH 8 tris buffer (55 mM) containing 50 mM NaOAc for the Capto Adhere column runs. Buffer exchanged mAbs were measured for their absorbance on a NanoDrop UV spectrophotometer, converted to concentration using a calibration curve, and then diluted to a concentration of 5 mg/ml for mAb A and to 4 mg/ml for mAb B.

3.4. Batch adsorption experiments

Batch isotherm data were generated on a TECAN™ EVO 200 using the Capto MMC resin with mAb A and Capto Adhere resin with mAb B. Resin slurry (50% v/v) was dispensed into 96-well plates using the robotic liquid-handling system and incubated with previously buffer exchanged mAb (varying pH and salt concentration) at protein fluid phase concentrations up to 6.67 mg/ml for mAb A and 1.67 mg/ml for mAb B. Incubation was performed for 60 min with shaking at 1100 rpm or 1250 rpm. Sodium acetate (20 mM) was used as the base buffering component between pH 5 and 6 (pH 5, 5.25, 5.5 and 6) with sodium chloride concentrations ranging from 20 mM to 650 mM for mAb A. Tris (55 mM) at pH 8 was used as the buffer with sodium acetate concentrations ranging from 50 mM to 650 mM sodium acetate for mAb B. Load densities (mass of protein incubated per volume resin) between 5 and 160 mg/ml were used to generate isotherms at each mobile phase condition, resulting in 4–7 points per isotherm. Resin volume in Capto MMC batch experiments was adjusted to allow for higher resin loading, with the smallest amount of resin used being 12.5 ul and the fluid phase being consistently 300 ul (liquid/solid volume phase ratio of 24). Resin volume in Capto Adhere batch experiments was also adjusted to allow for loadings, with the smallest amount of resin used being 2.5 ul and the fluid phase being consistently 240 ul (liquid/solid volume phase ratio of 96). Reproducibility of the batch experiments was validated by performing several high loading conditions in duplicate. MAb solid phase concentration q_p was calculated via mass balance with inclusion of hold-up volume effects [12], where the resin hold-up volume was used as three-fifths of the total solid phase volume (an internal heuristic). Concentrations were determined by either using the Lunatic™ microfluidic system or a plate reader. Two versions of the batch data were used, one including all native loadings, batch full isotherm (BFI), and the other having removed points corresponding to the linear region of the isotherm, batch no linear (BNL). The linear region was defined as all data points with mAb concentration less than 15% of the maximum liquid phase protein load concentration without exception. This cutoff was selected due to its consistent visual correspondence to the initial slope of the batch data for both resins and mAbs.

3.5. Column linear salt gradient elution experiments

Salt linear gradient elution (LGE) experiments were run at 0.2 ml/min on a 1 ml Capto MMC column (5 min residence time) and at 0.4 ml/min on a 1 ml Capto Adhere column (2.5 min residence time) using an ÄKTA Explorer 10 equipped with a 2 mm UV flow cell. Load densities of 25 mg/ml were employed for Capto MMC with mAb A and 20 mg/ml for Capto Adhere with mAb B. Each LGE experiment for Capto MMC was performed with a 20 mM acetate buffer at a different pH (5.3, 5.6, 5.9, and 6.2) using a 30 CV gradient from 0 to 1.5 M NaCl followed by a 20 CV hold at 1.5 M NaCl and a 10 CV strip using 0.1 M tris base. Each LGE experiment for Capto Adhere was performed with tris buffer at different gradient lengths (5, 10, 20, and 30 CV) at pH 8 from 0 to 1 M NaOAc followed by a 20 CV hold at 1 M NaOAc and a 10 CV strip using 0.2 M acetic acid. In both cases the column was regenerated for 10 CV with 0.5 M NaOH and re-equilibrated with the starting buffer until constant pH was reached. Following run completion, the UV 280 nm trace (mAU) and conductivity profile (mS/cm) were converted to units of concentration, mg/ml of mAb and molarity of salt counterion, respectively.

3.6. Chromatography system calibration

Calibration curves for the UV absorbance detector were generated using the method described by Kumar et al. [63]. First, a series of 2 ml samples, containing different concentrations of mAb A or mAb B between 0.5 mg/ml and 10 mg/ml, were injected into the ÄKTA system. The UV response at 280 nm was fit against the sample concentration using a second-order polynomial to ensure that the detector nonlinearity in the higher concentration range was accounted for. This calibration curve was later employed to convert the UV absorbance traces from the column experiments to units of concentration (mg/ml). Salt concentrations ranging from 0 M to 1.5 M NaCl in 0.1 M steps were pumped through the ÄKTA system using each buffering system (pH 5.3, 5.6, 5.9, and 6.2). For the tris buffer, salt concentrations ranging from 0 M to 1 M NaOAc in 0.1 M steps were employed. Conductivity measurements were fitted against the input salt concentrations with second-order polynomials for each buffering system. These calibration curves were used to verify the outlet salt concentration profiles for assurance that the gradients were performed as intended. Dead volume V_{dead} (from injection valve to UV detector) was determined via peak retention of an acetone injection (2% v/v) without the column in-line and determined to be 0.16 ml. The residence time of the salt gradient mixer was calculated by dividing the mixer size (0.6 ml) by the flow rate used in the column experiments. This parameter was later used as a simulation input to model the linear salt gradient with the approach outlined by Kumar et al. [64].

3.7. Determination of column parameters

Interstitial and intraparticle porosities were determined using the retention volumes of large (2 MDa dextran) and small (acetone) non-binding tracers. Ionic capacity Λ was calculated via column frontal loading and elution of small, UV-responsive, monovalent tracers. This method, similar to the histidine-based adsorber quantification method shown by Huuk et al. [56], was selected over the traditional potentiometric titration methodology [65] in order to avoid degradation of column packing that can arise during potentiometric titration due to the contact of deionized water [56]. Arginine (25 mM) was instead selected as the tracer due for Capto MMC, while 25 mM sodium nitrate was selected for Capto Adhere. To perform the quantification, the column was first flushed with 0.5 M HCl until completely equilibrated to remove all counterion species. Once the pH was stable, the respective tracer was fed through the column, monitored at UV 220 nm [66] for arginine and at 300 nm for nitrate [67], until 100% breakthrough was reached (absorbance plateau). Ionic capacities were determined by mass balance using Eqs. (19) and (20),

$$m_{ads} = m_{eluate} - \varepsilon_t V_{col} c_{load} - V_{dead} c_{load} \tag{19}$$

$$\Lambda = \frac{m_{ads}}{V_{col}(1-\varepsilon_t)} \tag{20}$$

Table 1
Values for column and resin parameters for Capto MMC. Values marked with [a] were taken from Zhu and Carta [68]. Values marked with [b] were taken from Roberts et al. [69].

	ε_e [−]	ε_p [−]	Λ [M]	d_p [μm]	r_{pore} [nm]
Capto MMC	0.37	0.916	1.513	85[a]	32[a]
Capto Adhere	0.40	0.913	2.153	75[b]	36[b]

where the mass of adsorbed tracer m_{ads} was calculated from the difference between the mass of tracer in the eluate m_{eluate} and the mass held up in the column. Here, ε_t represents the total porosity of the column. Mass of tracer in the eluate was calculated from integration of the elution peak with absorbance converted to mass based on the known load concentration c_{load} and the absorbance of the breakthrough plateau, assumed to correspond to c_{load}. Ionic capacities were then calculated by dividing the mass of adsorbed tracer by the equivalent solid phase volume and agreed with the ranges (accounting for ε_t) provided by the manufacturer for both resins. Finally, values of particle diameter and pore size, used for transport parameter correlations, were gathered from the literature [68,69]. Values for porosity, ionic capacity, particle diameter d_p, and pore size r_{pore} are shown in Table 1.

3.8. Isotherm parameter fitting

Isotherm parameter fitting was performed using IsoFit (https://github.com/alters9595/IsoFit), an open-source MATLAB-based software package for fitting of batch adsorption data developed recently by our group. This software allows for modular input of batch isotherm data (either single component or multicomponent) along with selection of a wide array of isotherm formalisms and other settings to help expedite the fitting process. After running the script for the primary module, all parameters are simultaneously regressed from the batch data using global optimization. Upon completion, goodness-of-fit statistics are calculated and provided to the user along with plots of the fitted isotherm data. IsoFit is free to use, and the reader is encouraged to use it for their own purposes. The software was coupled with a parallel tempering global optimization algorithm [70], code graciously provided by the University of Delaware, to perform fits. Batch isotherm data were collated in Microsoft® Excel® datasheets and imported into MATLAB® 2021a. The fitting was performed using a 16-core Ryzen 5950X processor (AMD®). Solid phase concentrations were converted into units per stationary phase volume by dividing by (1 – total porosity ε_t). This conversion was made to provide consistency in units of the equilibrium isotherm equations and the column simulations discussed in Section 3.10 [30]. Isotherm equations were assembled by converting them to their equilibrium form (setting left hand side to zero) and solved using the fsolve function (nonlinear function solver) in MATLAB. Isotherm parameters were determined via fitting to the mAb A – Capto MMC or mAb B – Capto Adhere batch data across all pH and salt concentrations simultaneously. Fitting was repeated twenty times for each isotherm formalism described in Section 2.2 to obtain a distribution of isotherm parameters for each model. Since the global optimization techniques employed in this study are non-deterministic (result depends on the random seed), the repeated fits (repeats) were necessary in order to provide confidence in the regressed isotherm parameters—the values of the parameters were different for each repeat. Fits were done for the entire range of loading, batch full isotherm (BFI), in addition to a constrained dataset where the points in the linear region of the isotherm, where liquid phase concentration was less than 15% of the maximum liquid phase load concentration, were removed, batch no linear (BNL). Reference pH values were set to 5.5 for Capto MMC to provide consistent scaling of the pH-dependent isotherm parameters. MAb B and Capto Adhere was only modeled at pH 8, so the pH-dependent isotherm parameters were not included.

Objective functions were calculated from the normalized root-mean-square error (NRMSE) between the simulated solid phase concentration $q_{k,sim}$ and the corresponding experimental value $q_{k,exp}$ for the k^{th} data point in the batch dataset. The objective function was then scaled by an empirically determined weighting coefficient W_k of 0.05 to yield an initial objective value close to unity, which was helpful for consistency in optimizer convergence. To prevent uneven weighting of any mobile phase condition (salt concentration at a given pH), due to each condition not necessarily having an equal number of data points, an additional weighting scheme, incorporated into W_k, was imposed to scale the weight of each data point by the total number of data points per each mobile phase condition. The overall objective function formulation is shown in Eq. (21),

$$\hat{\theta} = \arg\min_{\theta} \left(\frac{1}{N} \sum_{k=1}^{N} W_k \left(q_{k,sim} - q_{k,exp} \right)^2 \right) \tag{21}$$

where $\hat{\theta}$ is a given set of isotherm parameters and N is the number of data points. To expedite the fitting routine, simulated solid phase concentrations were calculated in parallel, using the Parallel Computing Toolbox™ in MATLAB (parfor function), before assembly into the overall objective value. Parameter bounds and initial guesses of each parameter value were given as additional inputs into the optimization routine. The parallel tempering algorithm was found to be highly robust with respect to parameter bounds and initial guess values, i.e., it was able to reach similar objective minima regardless of initial guess in a specified parameter search range. Optimization trajectories were populated in real-time and intermittently monitored to ensure progression. Isotherm fits (for those shown in this paper as well as those not shown) for both resins are provided in the supplementary material Excel datasheet.

3.9. Estimation of transport parameters

A key component of the column simulations was the input of transport parameters. The full GRM requires input of D_{ax}, k_{film}, D_p, and D_s for protein and salt components. D_{ax} was calculated using Eq. (22) [53],

$$D_{ax} = \mathrm{HETP} \frac{u}{2\varepsilon_e} \tag{22}$$

where the height-equivalent theoretical plates (HETP) were determined from peak area integration of the dextran UV trace, discussed in Section 3.7. D_{ax} was also calculated from the Péclet number (to provide a comparison with HETP-derived values), estimated using the correlation provided by Rastegar and Gu [71], which yielded a similar value to that obtained from the dextran peak. k_{film} was estimated using the Wilson-Geankopolis correlation Eq. (23) [72].

$$\mathrm{Sh} = \frac{1.09}{\varepsilon_e} \mathrm{Re}^{0.33} \mathrm{Sc}^{0.33} \tag{23}$$

Here, Sh, Re, and Sc refer to the Sherwood, Reynolds, and Schmidt dimensionless numbers, respectively, shown in Eq. (24).

$$\mathrm{Sh} = \frac{k_{film} d_p}{D_0}, \quad \mathrm{Re} = \frac{\rho u d_p}{\eta}, \quad \text{and } \mathrm{Sc} = \frac{\eta}{\rho D_0} \tag{24}$$

Determination of the dimensionless terms requires input of the particle diameter d_p, molecular diffusivity D_0, fluid viscosity η, and density ρ. D_0 was calculated using the Stokes-Einstein equation and effective pore diffusivity D_p of mAb was estimated using Eq. (25) [73].

$$D_p = \frac{\varepsilon_p D_0}{\tau_p} \psi_p \tag{25}$$

Table 2
Values for transport parameters of NaCl and mAb A with Capto MMC, NaCl and mAb B with Capto Adhere.

	NaCl		mAb A / mAb B	
	D_{ax} [mm^2/s]	k_{film} [mm/s]	D_p [mm^2/s]	k_{film} [mm/s]	D_p [mm^2/s]
Capto MMC	0.3142	0.1035	9.461×10^{-4}	1.159×10^{-2}	8.240×10^{-6}
Capto Adhere	0.2627	0.1213	9.358×10^{-4}	1.358×10^{-2}	2.840×10^{-5}

Here, τ_p is the resin pore tortuosity, whose value is uncertain but ranges between two and six [74], and was thus set to four. Further, ψ_p is the diffusional hindrance coefficient which was calculated using Eqs. (26) and (27) [75,76],

$$\psi_p = (1-\lambda_m)^{-2}\left(1+\frac{9}{8}\lambda_m \ln\lambda_m - 1.539\lambda_m\right) \quad \text{for } \lambda_m < 0.2 \tag{26}$$

$$\psi_p = 0.865(1-\lambda_m)^2\left(1-2.1044\lambda_m+2.089\lambda_m^3-0.984\lambda_m^5\right) \quad \text{for } \lambda_m > 0.2 \tag{27}$$

depending on the value of λ_m, calculated via $\lambda_m = r_{mAb}/r_{\text{pore}}$. MAb hydrodynamic radius r_{mAb} was set to 4.5 nm [77]. D_p for NaCl was instead estimated using the Mackie-Meares correlation Eq. (28),

$$D_p = \left[\frac{\varepsilon_p}{2-\varepsilon_p}\right]^2 D_0 \tag{28}$$

which is valid for small solutes [54].

Once all transport parameters had been estimated, an investigative approach was taken to ascertain their suitability for the LGE experiments with column simulations, approach outlined in Section 3.10, using the fitted isotherm parameters. To this end, brief column simulation sampling routines for k_{film}, D_{ax}, and D_p were performed for each isotherm model using the isotherm parameters resulting from their best fits to the batch data. The values of these transport parameters obtained from the correlations were used as initial guesses and a search space within an order of magnitude was utilized along with a simulated annealing algorithm. Fast convergence (less than a hundred iterations) of this algorithm allowed for relatively quick estimates of each transport parameter while gaining insight on their relative influence to the column simulations. k_{film} and D_{ax} were found to be minimally impactful on the simulated profiles, while D_p had a substantial effect for every isotherm model. This observation is consistent with the well-known heuristic that pore diffusion tends to be the limiting transport mechanism for protein-resin chromatography [32]. Thus, the correlated values of k_{film} and D_{ax} were selected while D_p was obtained via averaging of the sampled values for each model, resulting in a single universal set of transport parameters, shown in Table 2. Intriguingly, the D_p value for Capto Adhere was roughly 3.5 times greater than the value for Capto MMC, despite the pore sizes for the stationary phases being similar [68,69]. The reason behind this is speculative, but a possibility is that the lower binding affinities at low salt concentrations for Capto Adhere compared to Capto MMC in this study could result in faster diffusion rates due to a greater influence of solid diffusion (intraparticle diffusion in the adsorbed state) [78]. It is important to note that this method of transport parameter estimation serves to obviate the impact of the isotherm formalism, since no other parameters were changed between simulations of the same experiment. In this way, the transport parameters essentially acted as column model hyperparameters for each isotherm formalism. Other approaches to elucidate the relative contributions of the transport parameters could also be taken, such as using the HETP equation derived from the general rate model [53].

3.10. Column linear gradient simulations

Column simulations were performed using the ChromX™ (GoSilico GmbH, Karlsruhe, Germany) [79] simulation software, license graciously provided by GoSilico, using the GRM. The discretization scheme used was a linear streamline upwind Petrov-Galerkin (SUPG) finite element system in space using forty axial and ten radial nodes along with a fractional step theta scheme in time. Customized isotherm models, in their kinetic forms, were implemented into the software using provided templates. Simulations were executed using MATLAB front-end to automate the simulations. In this process, fitted isotherm parameters for each formalism were inserted into the simulation template and coupled with the column and transport parameters, allowing simulations to be run in an integrated manner. This strategy was employed for all twenty isotherm parameter fits, resulting in twenty sets of column simulations for every isotherm model for both BFI and BNL datasets for each resin. Visualization of predictions and their comparison to experimental data was performed using MATLAB. Column predictions (for those shown in this paper as well as those not shown) for both resins are provided in the supplementary material Excel datasheet.

3.11. Statistical analysis of batch data fits and column simulations

To determine the overall quality of batch data fits and column predictions, score metrics were created for interpretability. Batch data scores $\text{Score}_{m,r,B}$ were generated using Eq. (29),

$$\text{Score}_{m,r,B} = 1 - \left(\frac{\text{NRMSE}_{m,r}}{\text{NRMSE}_{\max}}\right) \tag{29}$$

where normalized (by the data mean) root-mean-squared error $\text{NRMSE}_{m,r}$ was calculated for each repeat r of each model m and again normalized based on the maximum NRMSE value $\text{NRMSE}_{\max}$ in the set of all twenty repeats for all models.

Column prediction scores $\text{Score}_{m,r,C}$ were generated using Eq. (30),

$$\text{Score}_{m,r,C} = 1 - \left(x_1\frac{\text{NRMSE}_{m,r}}{\text{NRMSE}_{\max}} + x_2\frac{\Delta\text{FM}_{m,r}}{\Delta\text{FM}_{\max}} + x_3\frac{\Delta\text{PW}_{m,r}}{\Delta\text{PW}_{\max}} + x_4\frac{\Delta\text{PM}_{m,r}}{\Delta\text{PM}_{\max}}\right) \tag{30}$$

which includes NRMSE in addition to three metrics describing the elution peak: first moment $\text{FM}_{m,r}$, peak width (at 95% confidence) $\text{PW}_{m,r}$, and peak maxima $\text{PM}_{m,r}$ with weights x_1, x_2, x_3, x_4, respectively. Δ of these metrics represents the deviation between the simulated value and experimental value. Values of these weights are set to 0.5 for NRMSE and $0.1\bar{6}$ for each peak metric, such that NRMSE accounts for half of the score while the peak metrics evenly compose the remaining portion. The column prediction score was assembled as such to provide a more realistic depiction of simulation agreement with the experimental data and is similar to the scoring strategy developed by Heymann et al. [80]. Resulting scores for batch fits and column predictions are bounded between zero and unity, with the worst candidate having a score of zero and a perfect candidate (zero error) having a score of unity. It is worth noting that the logarithm (base ten) of the NRMSE terms was instead employed for the Capto Adhere data set because the

spread in NRMSE values between the best and worst performing models was so broad that it entirely obscured differences in score between comparable models.

After calculation of the ensemble of scores for each model, the Akaike information criterion (AIC) [81–83] was employed to qualify the isotherm models based on their relative performance and their complexity (number of isotherm parameters). Eq. (31)

$$\mathrm{AIC}_m = R\ln\left(\frac{1}{R}\sum_{r=1}^{R}(1-\mathrm{Score}_{m,r})^2\right) + 2P + \frac{2P(P+1)}{R-P-1} \tag{31}$$

shows the formulation of the AIC used in this study, where the first term represents the log likelihood function and is composed of the log residual of the scores, for either the batch fits or the column predictions (using the same equation). Here, P is the number of isotherm parameters and R is the number of repeats performed. It is worth noting that the first term includes the sum of all score residuals and thus should account for the spread in score values within a set of repeats for a given model, which may vary notably with model complexity. The second term represents the negative weight (since a larger value of AIC indicates a lower ranked model) associated with the number of parameters. Further, a correction for small sample size ($R/P < 40$) is applied in the third term. Next, the AICs are rescaled to Δ_m using Eq. (32)

$$\Delta_m = \mathrm{AIC}_m - \mathrm{AIC}_{\min} \tag{32}$$

to improve their interpretability by subtracting the lowest AIC of all models $\mathrm{AIC}_{\min}$ from all AIC_m. This results in the model with the lowest AIC having a Δ_m of zero and thus being the highest ranked. Lastly, Eq. (33)

$$w_m = \frac{\exp(-\Delta_m/2)}{\sum_{m=1}^{M}\exp(-\Delta_m/2)} \tag{33}$$

is used to calculate the model likelihood w_m (Akaike weight), which represents the probability of selecting a model, from Δ_m for all models M. This equation results in each model having a score between zero and one, such that the sum of all w_m is unity.

3.12. Isotherm parameter sensitivity analyses

Sensitivity analyses were performed using the elementary effects method, also called one-at-a-time (OAT) analysis or the Morris method [84]. Briefly, this method is an iterative process where each parameter (isotherm parameter) is separately perturbed by a fixed percentage to develop a sampling matrix for each model. Twenty fixed percentages (0.1% to 2% in 0.1% steps) were employed in this work to obtain confidence in the analyses. The first row of this matrix corresponds to the native (unperturbed) set of isotherm parameters and each subsequent row corresponds to the same set with a single perturbed isotherm parameter. Next, isotherms and column simulations were generated using the isotherm parameters present in each row. Variances corresponding to each parameter and model, for batch and column, were then calculated using the root-mean-square error between the simulation with the native parameters and the simulation with a perturbed parameter. Lastly, sensitivity scores were calculated via the ratio of individual parameter variances to the total sum of parameter variances for each model. A more detailed description of this method along with its mathematical construction is provided in SI.2 (Word document)

4. Results and discussion

4.1. Model selection workflow

The objective of this work was to rigorously examine the relative efficacies of various isotherm formalisms for their ability to use batch isotherm data to make direct column predictions for Capto MMC, a multimodal cation-exchange resin, and for Capto Adhere, a multimodal anion-exchange resin using two mAbs (mAb A and mAb B). To this end, a workflow (Fig. 1) was employed to qualify the isotherm models using various techniques of inspection.

Briefly, the workflow was initiated with determination of isotherm parameters for seven isotherm formalisms and two data subsets (corresponding to selected loading conditions) via fitting of batch isotherm data. Importantly, fitting was repeated twenty times for each model to characterize their reproducibility. Isotherm parameters for all models are included in SI.1 Table 1 for Capto MMC – mAb A and in SI.1 Table 2 for Capto Adhere – mAb B, along with confidence intervals for each parameter based on their 95% significance level between the twenty fits. Column and stationary phase parameters were either determined experimentally or obtained from the literature. Transport parameters were then calculated primarily using physical correlations based on operational parameters as well as parameters describing the columns, stationary phases, and the mAbs. Overall sets of isotherm, column, and transport parameters were thereafter employed to perform column simulations using the general rate model framework. Isotherm models were next compared with respect to their relative abilities to predict the elution curves, where evaluation was based on both visual inspection (agreement between simulation and experimental data) and statistical methods. The Akaike information criterion was employed as a statistic to aid in model selection and sensitivity analyses were lastly performed to provide further insight into the relative contributions of each isotherm parameter.

4.2. Influence of batch data loading conditions on model performance for Capto MMC

Column simulations for Capto MMC using the pH dependent SMA isotherm with parameters obtained from BFI data (no batch data points removed) are shown in Fig. 2. As can be seen, the SMA BFI simulations were not in good agreement with the experimental column data. While the peak center of mass was roughly aligned at the lower two pH values 5.3 (Fig. 2A) and 5.6 (Fig. 2B), this comparison worsened for the higher two pH values 5.9 (Fig. 2C) and 6.2 (Fig. 2D). Further, the simulated peak shapes were significantly broader than those obtained in the experiments. The variability between repeated isotherm fits can also be evaluated from these simulations. For this isotherm, there were minimal differences between the worst, median, and best column predictions obtained from repeated batch isotherm parameter fits. Interestingly, while the column simulation results with this isotherm model were subpar, the batch data were well-fitted across all salt and pH conditions, illustrated by the fits at pH 5.25 and 6 (Fig. 2E, 2F). This disparity indicates that the quality of the batch data fit may not be a sufficient determinant of column simulation accuracy. Future work will examine this in more detail to determine if there are certain heuristics that can improve the connectivity between the batch and column fits.

While the SMA isotherm did not show adequate results with the BFI data, column simulations with SMA isotherm parameters obtained from BNL batch data (without the linear portion) exhibited a significant improvement in their agreement with the experimental data (Fig. 2G–2J). Here, the simulated peaks became much better aligned at the lower two pHs, with similar peak shapes as those obtained in the experiments. This agreement decreased at higher pH, with misalignment of the peaks at pH 5.9 and 6.2. High consistency was also seen between the runs, with only minor differences seen between the median and best simulations at the higher pH values. When comparing the batch isotherm fits (Fig. 2E, 2F for BFI and Fig. 2K, 2L for BNL) one can see that the shapes are noticeably different. When the low concentration data points

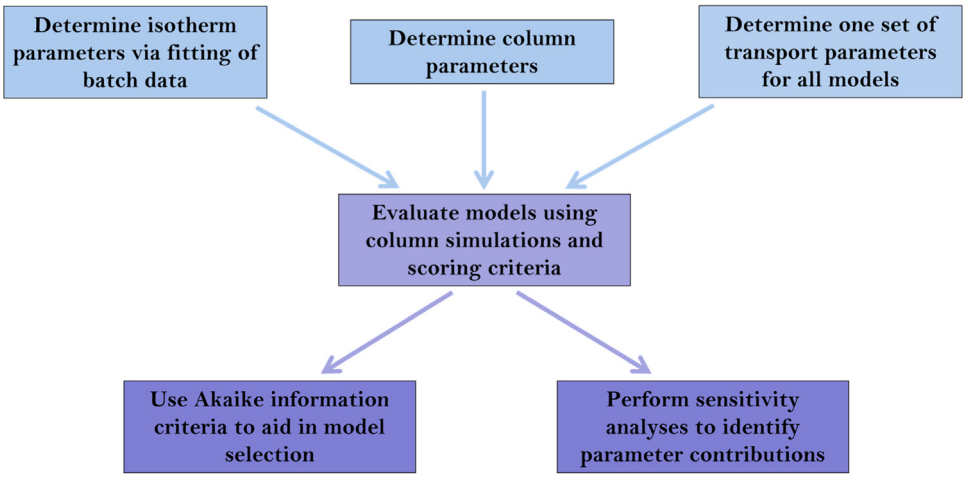

Fig. 1. Workflow describing the strategy for evaluation and selection of isotherm formalisms.

were removed (Fig. 2K, 2L), the initial slopes of the fits became significantly steeper, with the isotherms at low salt concentration becoming essentially square. This observation was accompanied by noticeable differences in the Capto MMC linear isotherm parameter values (SI.1 Table 1) between SMA BFI and BNL—equilibrium constants $K_{eq,0}$ and $K_{eq,1}$ are larger for BFI, while characteristic charges ν_0 and ν_1 are larger for BNL. As expected, the high concentration data were captured better by the BNL fit. This may imply that BNL outperformed BFI simply because it captures the plateau region of the batch data better, thus being more relevant to the high-load (25 mg/ml, ~60% of DBC) experimental conditions typical of process chromatography. Because elution under nonlinear loading conditions refers to the region of the adsorption isotherm where the protein concentration is high and the salt concentration is sufficient to result in elution, it is necessary to accurately capture this region of the batch data to obtain sound column predictions. Another contributing factor for this discrepancy is that the error-prone nature of the low concentration batch adsorption data could lead to a decrease in model quality, reflected in the accuracy of the column simulations. In scenarios of such high binding affinity with large initial slopes, small deviations in liquid phase protein concentration measurements may result in significant differences in calculated solid phase concentrations. With some of these data points having concentration values that were near zero, it is possible that intrinsic measurement errors during the batch experiments led to poor column predictions. Based on these results with SMA, BNL data were used for Capto MMC in visualizing predictions for the remaining isotherm models investigated in this study.

4.3. Comparisons between SMA and SMA K_S *models for Capto MMC*

A slightly modified version of the SMA model, SMA K_s, was next evaluated with respect to its ability to fit the batch data as well as to predict the elution profiles for Capto MMC. Here, a single parameter K_s (one of the Mollerup terms [50,51]) is added which allows the isotherm to have some added flexibility in its equilibrium constant via an exponential dependence on salt concentration. This modification helps address one of the key limitations of the classical SMA model, namely the fixed value of the equilibrium constant. As can be seen in the supplementary material Excel datasheet, this modification resulted in a significant improvement in the ability of the simulations to predict both peak shapes as well as the impact of pH on the elution behavior. Evidently, the decay in prediction accuracy with increasing pH is addressed, which can be attributed to the increased flexibility of the isotherm. Since the K_s term is positive, the decline in binding affinity with increasing salt occurs at a slower rate as compared to the base SMA model. This manifests in the peaks shifting to the right (as compared to the SMA model), particularly at the higher two pHs, enabling better characterization of the peak shape and retention. Although the column predictions were clearly improved, the batch isotherm fits were indistinguishable as compared to those of the unmodified SMA model. Again, this implies that the quality of the batch isotherm fit is often not an adequate predictor of the column behavior. One of the drawbacks, however, of the SMA K_s model is a decrease in the consistency between repeated simulations with the different parameter sets from the batch fits. This is an expected result since variability in parameter estimation tends to increase with model complexity. Notwithstanding, even the worst prediction for SMA K_s was comparable to the best prediction with SMA. These results demonstrate that the K_s modification is a clear improvement over the base SMA model for this scenario.

4.4. Influence of batch data loading conditions on model performance for Capto Adhere

Having demonstrated that BNL adsorption data resulted in improved predictions for Capto MMC, it was of interest to ascertain if this was also the case for Capto Adhere. As can be seen, the differences between BFI (Fig. 3A–3E) and BNL (Fig. 3F–J) predictions were not discernible for the SMA K_s model. The distinction in the effect of removing the low concentration data is associated with the shapes of the isotherms, where a stark difference is seen between the curves for Capto Adhere and Capto MMC batch data. The isotherm data shown for Capto MMC was highly favorable, with steep initial slopes in contrast with the shallow initial slopes shown for Capto Adhere. Measurement error is expected to be pronounced at low protein concentrations (near zero) and results in inaccuracies when these points are included in the model. However, for shallow slopes, batch data points at low protein loadings can be more reasonably measured. In this case, the predictions for BFI and BNL are similar enough that it is unclear if the low concentration should be removed. For the sake of experimental efficiency, necessitating fewer data points is ideal, however more complex isotherm models should be evaluated to conclude which data sets are ideal. Visualization of predictions for the remaining models studied for Capto Adhere here will be shown using BFI data for brevity (i.e., not using BNL data). Lastly, the magnitude of the isotherm parameters (SI.1 Table 2) obtained for BFI and BNL are similar, indicating that the nearly identical isotherm shapes are consistent with the parameter values. This observation is also in contrast with what was seen for Capto MMC, where there were

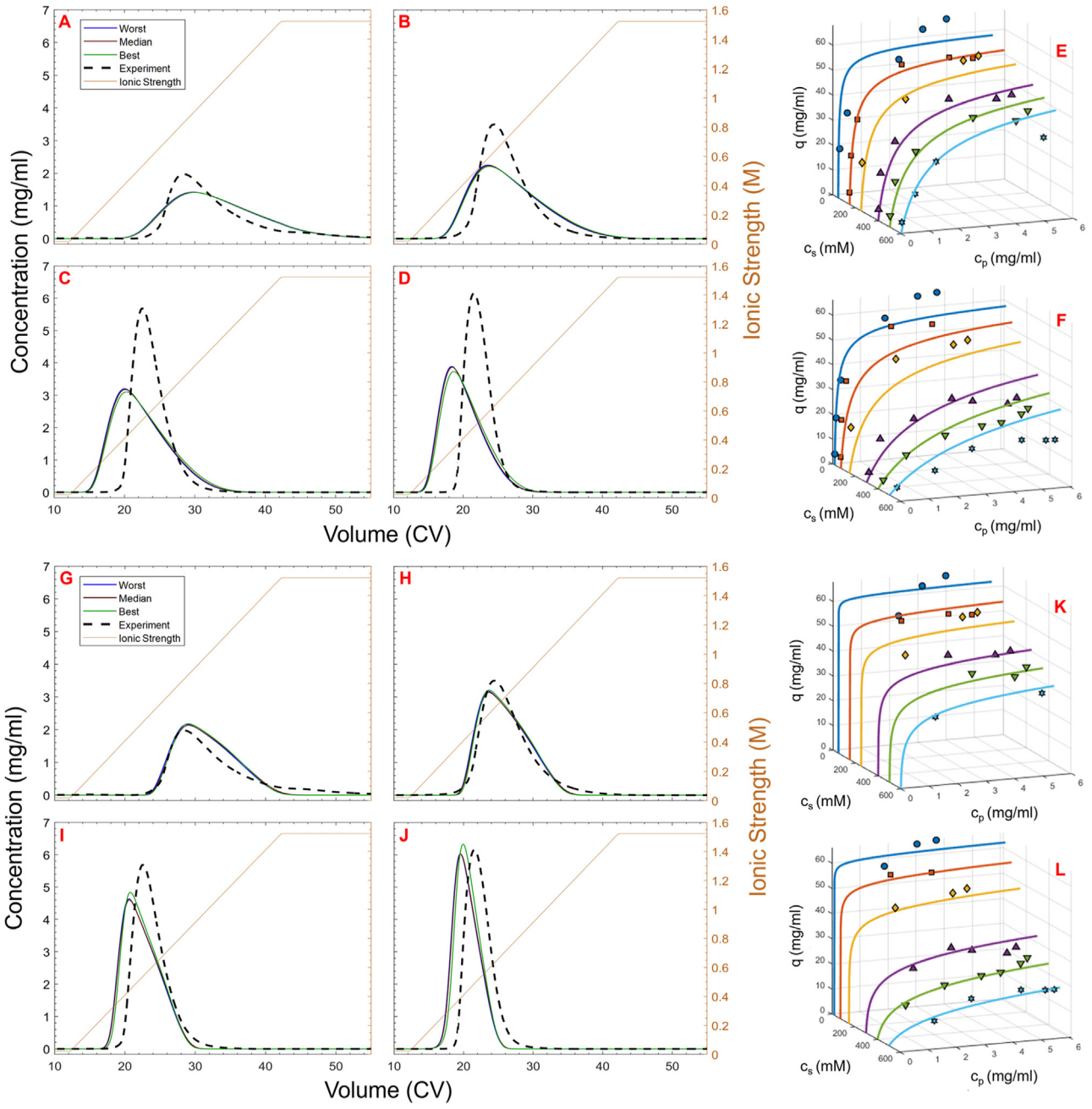

Fig. 2. Capto MMC column simulations and batch isotherm fits using SMA BFI. Simulations: (A) pH 5.3; (B) pH 5.6; (C) pH 5.9; (D) pH 6.2. Solid blue lines: lowest scoring prediction; Solid brown lines: median scoring prediction; Solid green lines: best scoring prediction; Dotted black lines: experiment. Batch isotherm fits: (E) pH 5.25; (F) pH 6.0. Simulations using SMA BNL: (G) pH 5.3; (H) pH 5.6; (I) pH 5.9; (J) pH 6.2. Batch isotherm fits: (K) pH 5.25; (L) pH 6.0. Note that the isotherm fits correspond to the best column predictions.

notable discrepancies in the magnitude of the linear isotherm parameters which were consistent with changes in the initial slopes.

4.5. Comparisons between SMA and SMA K_S *models for Capto Adhere*

While the SMA isotherm showed some promise for the Capto MMC resin, this was not the case for Capto Adhere. The results with the SMA model for Capto Adhere (provided in the supplementary material Excel data sheet) indicated, unequivocally, that it is unable to fit the batch data and to predict the column elution profiles. The decrease in elution recovery with decreasing gradient length (increasing gradient slope) is not predicted and the isotherm shape, with respect to ionic strength, is monotonic—which is clearly not correct. These observations are unsurprising in that the functional form of the SMA isotherm yields a strictly decreasing binding capacity with increasing salt concentration, making it unable to describe a U-shaped binding trend in the isotherms. This is an intrinsic limitation of the SMA model and demonstrates that more complex isotherm formalisms must be used for this scenario.

Column linear salt gradient simulations and fitted batch adsorption data using the SMA K_s model in BFI form are shown in Fig. 3A–3E. Column predictions are shown at four gradient lengths: 5 CV (Fig. 3A), 10 CV (Fig. 3B), 20 CV (Fig. 3C), and 30 CV (Fig. 3D), while the batch data fit is shown in Fig. 3E. In sharp contrast to the SMA isotherm, the SMA K_s model was able to capture both the isotherm and elution profile trends. As can be seen, the batch solid phase concentrations exhibited a more complex behavior with re-

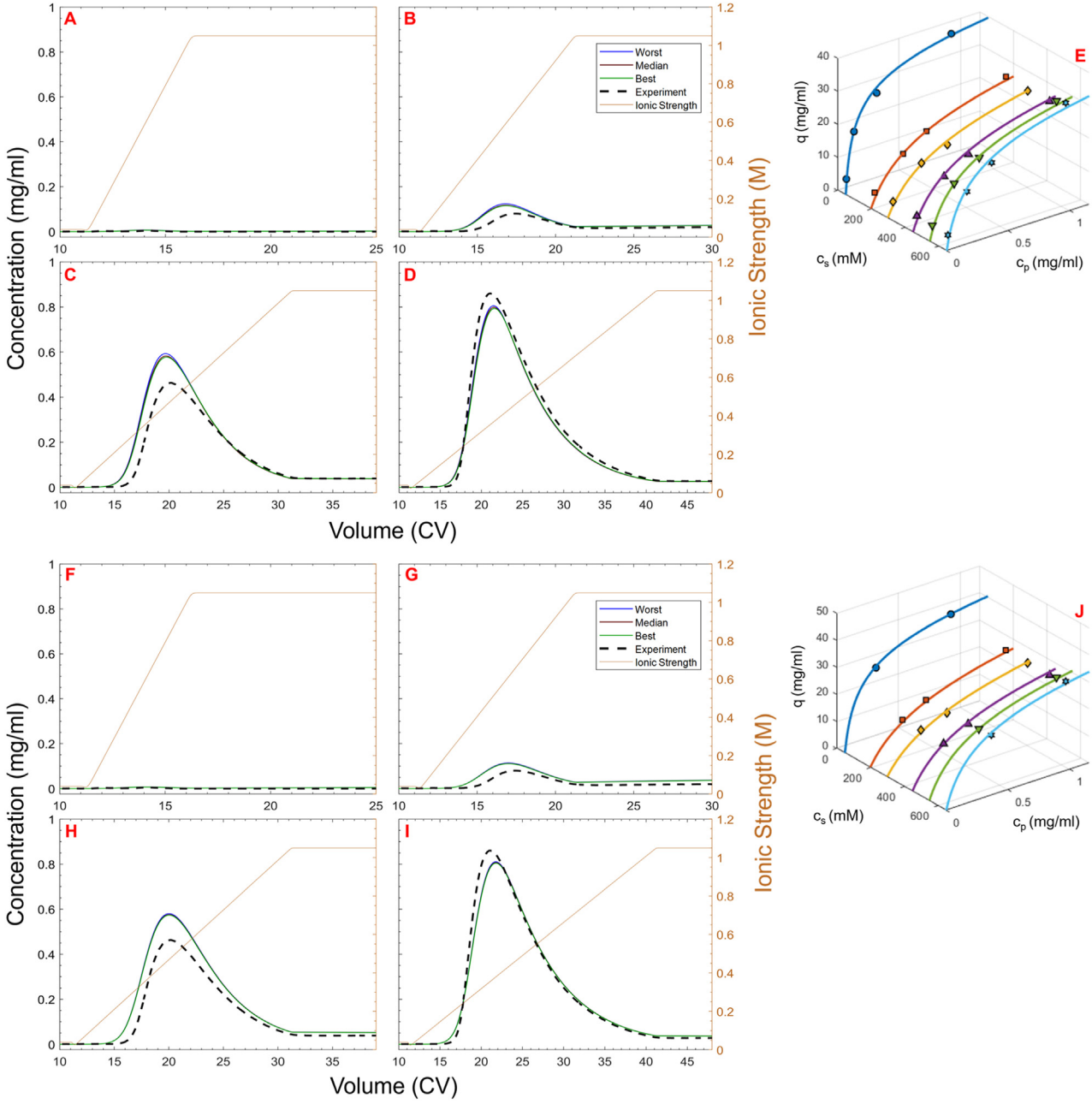

Fig. 3. Capto Adhere column simulations and batch isotherm fit using SMA K_s BFI. Simulations: (A) 5 CV gradient length; (B) 10 CV gradient length; (C) 20 CV gradient length; (D) 30 CV gradient length. Solid blue lines: lowest score predictions; Solid brown lines: median score predictions; Solid green lines: best score predictions; Dotted black lines: experiment. Batch isotherm fit: (E) pH 8.0. Simulations using SMA K_s BNL: (F) 5 CV gradient length; (G) 10 CV gradient length; (H) 20 CV gradient length; (I) 30 CV gradient length. Batch isotherm fit: (J) pH 8.0. Note that the isotherm fits correspond to the best column predictions.

spect to salt concentration than was observed for Capto MMC. This included a U-shaped relationship of the adsorbed concentration with respect to ionic strength at both linear and non-linear adsorption conditions as well as a lack of a "non-binding" condition. This adsorption behavior is a result of the multiple modes of interaction present in the multimodal anion-exchange system, namely, electrostatic and hydrophobic interactions. Importantly, the U-shaped isotherm is associated with elution recovery losses in salt gradients at increasing gradient slopes. This trend is evident here—the peak completely disappeared when the gradient length is decreased to 5 CV. Surprisingly, the SMA K_s model, without any parameters explicitly associated with hydrophobicity, was able to accurately predict both the recovery loss and the narrowing peak shape with respect to gradient slope in the column simulations.

With a single modification (K_s), the flexibility of the SMA model was drastically increased with respect to its ability to account for this more complex salt dependent behavior. In fact, this model addresses one of the key limitations of the SMA model, namely that the equilibrium constant is fixed. While small positive values of K_s (< 0.5) determined for Capto MMC allowed for better prediction in the subtleties of peak shape (delayed elution and tailing), the large positive values (> 4) determined for Capto Adhere had a dramatic impact on the predicted profiles (growth in peak shape, tailing, and recovery loss). In addition to its significantly improved performance, the minimal number of parameters in the SMA K_s model allows it to readily fit the data while also achieving consistent predictions between repeats. Overall, this simple modification can be employed to notably improve the capabilities of

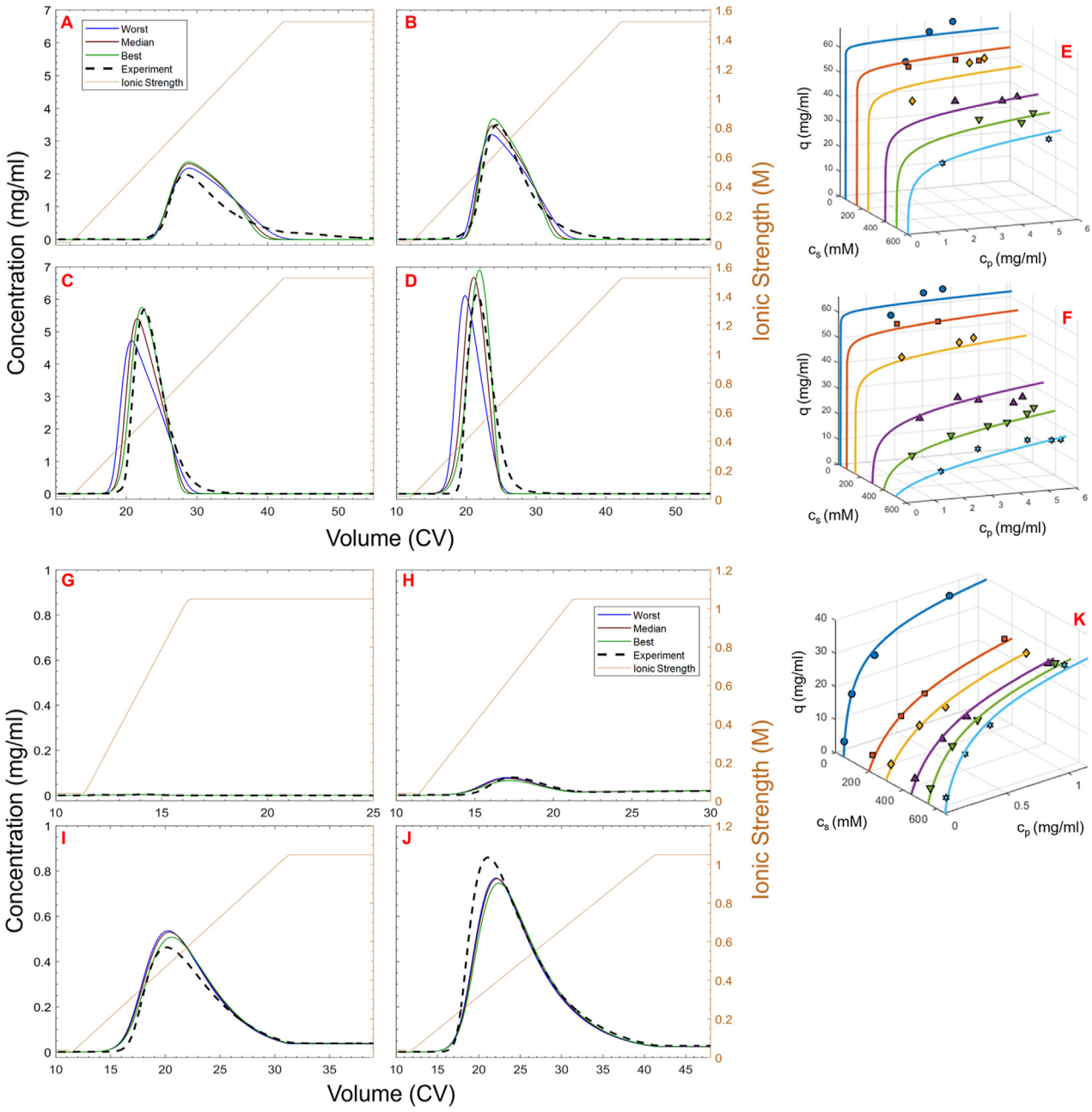

Fig. 4. Capto MMC column simulations and batch isotherm fits using SMA Ext. BNL. Simulations: (A) pH 5.3; (B) pH 5.6; (C) pH 5.9; (D) pH 6.2. Solid blue lines: lowest scoring prediction; Solid brown lines: median scoring prediction; Solid green lines: best scoring prediction; Dotted black lines: experiment. Batch isotherm fits: (E) pH 5.25; (F) pH 6.0. Capto Adhere column simulations and batch isotherm fit using SMA Ext. BFI. Simulations: (G) 5 CV gradient length; (H) 10 CV gradient length; (I) 20 CV gradient length; (J) 30 CV gradient length. Batch isotherm fit: (K) pH 8.0. Note that the isotherm fits correspond to the best column predictions.

the original SMA model to describe significantly more complex behavior.

4.6. Comparisons with extended SMA model

As described in the theory section, the SMA K_s model can be expanded by including an additional term K_p (second Mollerup term) to create the SMA Extended (Ext.) isotherm. This K_p term differs from K_s in that it is tied to an exponential dependence on protein concentration instead of salt concentration, giving the isotherm additional flexibility, particularly in regimes of high protein loading. After adding this parameter, the accuracy of column simulations was seen to further improve for Capto MMC (Fig. 4A–4D), with the general peak shape and alignment in even closer agreement with the experimental data. Since the value of K_p was positive for all isotherm parameter fits, the effective binding strength was modified as the protein concentration increased, resulting in better agreement between the simulated and experimental profiles. As anticipated, the variability between repeat simulations increased for the SMA Ext. model due to its increased complexity. For the SMA Ext. batch isotherm fits (Fig. 4E, 4F), some differences, while subtle, can be seen in comparison to the SMA and SMA K_s models. The primary difference here being that the plateau region is slightly sloped upwards for the SMA Ext. model, which makes sense due to the presence of the K_p parameter adding an additional dependence of the isotherm shape on the protein concentration. Since SMA Ext. has both K_s and K_p, these two parameters can be tuned in conjunction to provide additional control

of the shapes of both the elution profiles and isotherm shapes through effective adjustments of the equilibrium constant. In fact, these parameters can be adjusted to account for a range of affinity vs. salt behavior, be it subtle departures from monotonicity as shown for Capto MMC, or to completely non-monotonic behavior, shown for Capto Adhere.

This model was also employed for Capto Adhere, where column simulations and the batch data fit are shown in Fig. 4G–4K, where a subtle improvement in the quality of predictions can be seen as compared to those obtained SMA K_s. This improvement is accompanied by a minor decrease in consistency between repeats. While the addition of K_p led to a noticeable improvement for the SMA model with Capto MMC, the impact here is not as significant. Since the influence of this parameter is tied to protein concentration and the concentration during elution is relatively low, the utility of K_p is minimized. With respect to the parameter values, similarities are seen between SMA Ext. and SMA K_s. Aside from the commonalities in fitted isotherm shapes, similarities in parameter values may imply that there are ideal ranges and combinations that are required to achieve sound predictions. Well-determined parameters (narrow confidence intervals) residing in the same range suggest that their magnitude can be an indicator of prediction success. This is important when adding additional parameters to the model since this tends to increase variability in fitted values (broader confidence intervals). If the added parameters do not contribute notably to model predictions, their addition may simply detract from the consistency that is provided from the essential parameters.

4.7. Comparisons with explicit multimodal isotherm formalisms

While the single-mode SMA-type isotherm models described above were well-performing overall (qualitatively), it was also of interest to examine isotherms with explicit (stoichiometric) hydrophobic contributions. Fig. 5A–5F shows the Capto MMC column predictions and isotherm fits obtained when using the Ottens Ext. model which is described in Nfor et al. [12]. As described in Section 2.2, this model has three additional parameters added (n_0, n_1, and s) to the SMA Ext. isotherm. These parameters account for the stoichiometry of hydrophobic interactions (analogous to ν_0 and ν_1) and the number of shielded hydrophobic binding sites (analogous to σ), respectively. Although the batch isotherm fits were similar to those obtained with the SMA-type model fits, the quality of the column predictions was quite different. Not only was the variability between different repeats more pronounced with Ottens Ext., but even the best prediction with this isotherm did not approach the predictions achieved with the SMA Ext. model. Apparently, adding these parameters seemed to decrease model robustness while not offering any noticeable benefit under these column conditions. As shown in SI.1 Table 1, the confidence intervals of n_0 and n_1 are much greater than those for ν_0 and ν_1, indicating that the charged stoichiometric terms are better determined than the hydrophobic stoichiometric terms for this isotherm. This suggests that n_0 and n_1 may not be appropriate parameters to include in the model framework for this application. By including parameters that have a relatively minor impact on the model output, the added complexity of the model can lead to variability in the parameter fitting routine without any clear advantage stemming from their addition. This point will be further elaborated on later in this work using sensitivity analyses of the individual isotherm parameters. We also examined the Ottens model in a reduced form, with the K_s and K_p terms removed ("Ottens" instead of "Ottens Ext."). The results demonstrated that the predictive ability of this form of the Ottens model was lower than the unreduced formulation and had the lowest performance of all models examined in this work (shown in the supplementary material Excel datasheet).

It is worth mentioning that removing the low concentration data (BNL) also improved predictions for Capto MMC with the multimodal isotherm formalisms. Hahn et al. [46] proposed that the use of a single adsorption capacity for both electrostatic and hydrophobic interactions in the Ottens Ext. model (Nfor et al. [12]) may have led to difficulties in capturing both the linear and nonlinear regions of the Capto MMC isotherms in this work. This reasoning is questioned by the Capto Adhere results in this study—while the assumption of simultaneous binding was applied for both Capto MMC and Capto Adhere, difficulties in describing both linear and nonlinear regions were not present for Capto Adhere. If the applied assumption was invalid, it would have resulted in these difficulties for both resins. Therefore, it is more likely that these difficulties arise from the inability to capture the isotherm shape with respect to loading concentration (steepness of the uptake region, i.e., favorability).

Further investigation of the Ottens Ext. isotherm model's capability to predict the elution behavior and to fit the batch data for Capto Adhere is shown in Fig. 5G–5K. While the n and s parameters are included in the model formulation to obtain a more realistic depiction of the hydrophobic components of the multimodal interactions—which are dominant in the U-shaped binding scenario—their inclusion, interestingly, did not seem to improve the model predictions. In addition, there was more variation between the set of repeats due to the larger number of parameters being fit, also indicated by the increase in confidence interval size for the parameters (SI.1 Table 2). Further, the simulations for the best repeat were quite similar to the results produced by the simpler isotherm models, suggesting that the n and s parameters did not offer any discernable benefit to the model formulation in this scenario. It is worth noting that the n value determined with this data for the Ottens Ext. model was quite small with an exceptionally large confidence interval, suggesting that the value was not well-determined and that it did not have a dramatic impact on the fit. Further, as shown in the supplementary material, removal of the K_s and K_p parameters from the Ottens Ext. model resulted in predictions that were even worse than those produced by the base SMA model, even with appreciable n values. This implies that the n and s parameters could not describe the influence of hydrophobic interactions in these systems without the presence of the activity coefficient parameters.

In addition to the Ottens models, another set of multimodal isotherm models, called SMAHIC and SMAHIC Ext., was investigated. This model differs from the Ottens construction—two parameters β_0 and β_1 are added to the model formulation. These parameters represent the number of released water molecules in the hydrophobic exchange reaction [62], with β_0 acting as a multiplicative constant and β_1 being tied to an exponential dependence on salt concentration. SMAHIC Ext. has these two parameters with K_s and K_p also present, resulting in a total model construction similar to the isotherm formalism presented by Lee et al. [16]. While this model presents a holistic depiction of the multimodal interaction, it has some potential redundancies in its parameters, wherein β_1 and K_s are both tied to an exponential dependence on salt. The only difference being that β is tied to n (present in the exponent for solid phase concentration) while K_s is tied to K_{eq}. Further, the SMAHIC Ext. model contains the greatest number of parameters (12) out of all the isotherms considered in this paper. Since the variability in column predictions increases with model complexity, there must be an advantage present for the more complex model to be selected. This in mind, parameter redundancy is undesirable as it can decrease model robustness and may not affect performance substantially. Prediction and fit results are shown in the supplementary material for the SMAHIC isotherm and in Fig. 6A–6F for the SMAHIC Ext. isotherm. While the SMAHIC model yielded one of the repeat runs achieving the most accurate single predic-

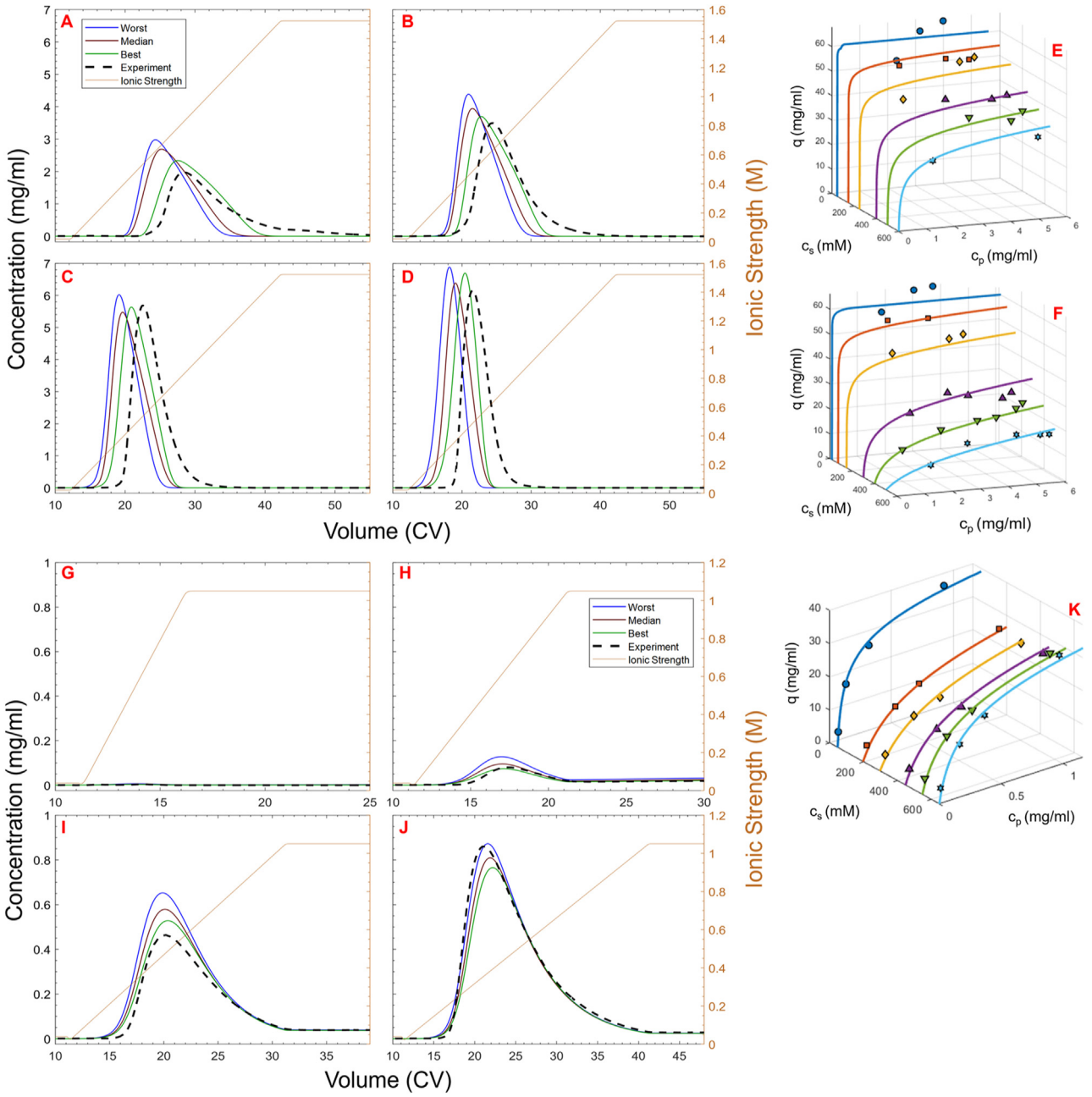

Fig. 5. Capto MMC column simulations and batch isotherm fits using Ottens Ext. BNL. Simulations: (A) pH 5.3; (B) pH 5.6; (C) pH 5.9; (D) pH 6.2. Solid blue lines: lowest scoring prediction; Solid brown lines: median scoring prediction; Solid green lines: best scoring prediction; Dotted black lines: experiment. Batch isotherm fits: (E) pH 5.25; (F) pH 6.0. Capto Adhere column simulations and batch isotherm fit using Ottens Ext. BFI. Simulations: (G) 5 CV gradient length; (H) 10 CV gradient length; (I) 20 CV gradient length; (J) 30 CV gradient length. Batch isotherm fit: (K) pH 8.0. Note that the isotherm fits correspond to the best column predictions.

tion out of all the models studied, this success was overshadowed by the variability of the predictions. The high accuracy of the best repeat run could be attributed to having interactions between the multiplicative β and n terms that allowed for an increase in the flexibility of the functional form. Although reasonable predictions were produced with the SMAHIC Ext. model, there was no clear improvement over the simpler models. This seems to imply that there is no benefit for including both K_s and the β terms in the model framework. The overall contribution of hydrophobic interactions is evidently minimal, for the range of salt and pH conditions investigated, so the results presented here for MMCEX are not surprising. While the hydrophobic interactions do result in increased salt tolerance, compared to single mode ion-exchange systems, the relationship of binding affinity to salt concentration is purely monotonic in the MMCEX system which suggests that explicit hydrophobic terms are not required. Conversely, while the contribution of hydrophobic interactions for Capto Adhere is more significant, these isotherm parameters still do not provide any noticeable benefit.

Predictions with the SMAHIC (shown in the supplementary material Excel datasheet) and SMAHIC Ext. (Fig. 6G–6K) models were also performed for Capto Adhere. Evidently, adding the β_0 and β_1 parameters into the model formulation led to a significant drop in predictive ability. This result is striking—the best repeat could no longer capture the shape or retention of the elution peaks, while the prior models could. Possible contributing factors to the lackluster performance of the SMAHIC Ext. model could be variability in parameter fitting, nonintuitive interactions between parameters,

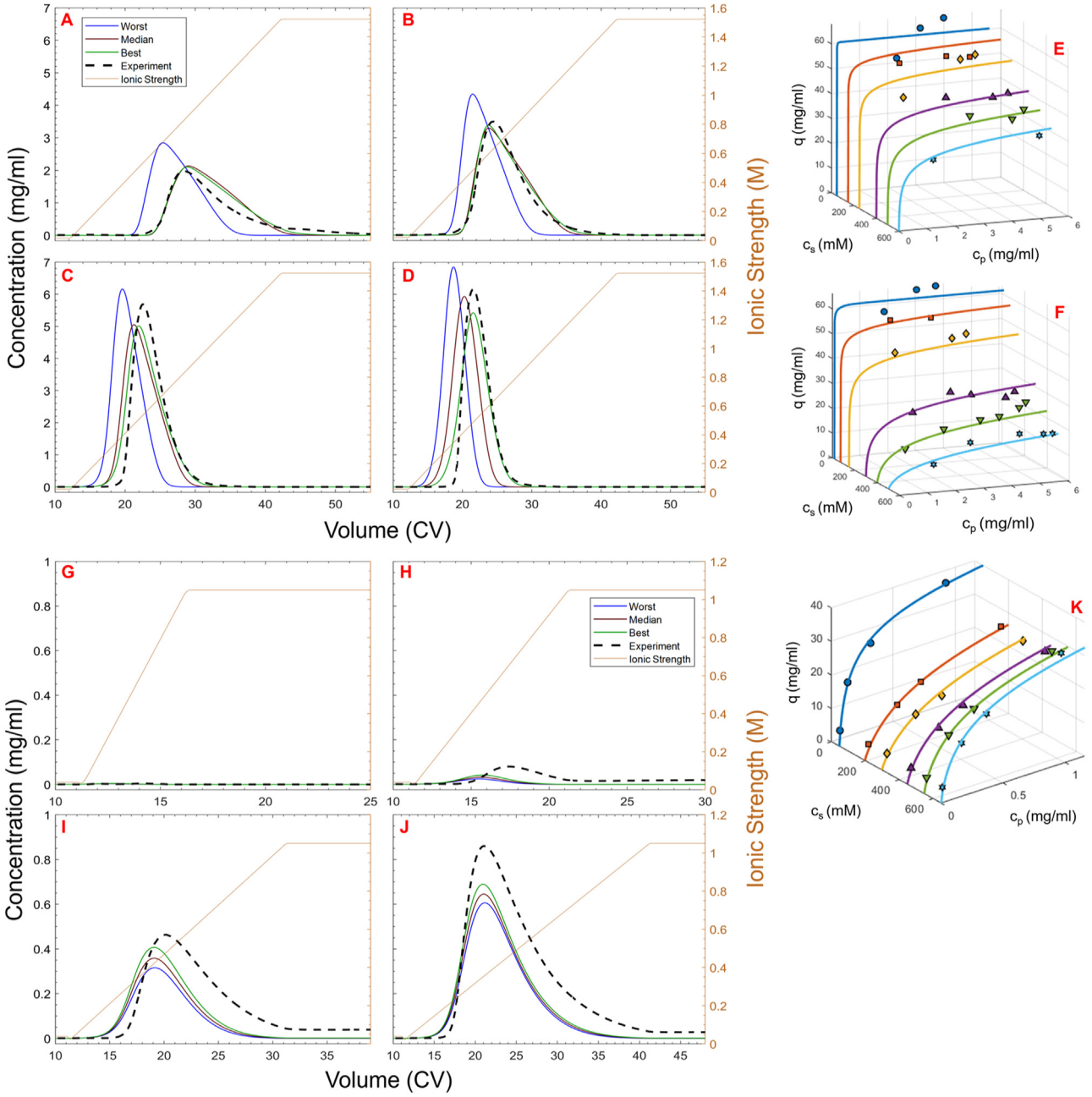

Fig. 6. Capto MMC column simulations and batch isotherm fits using SMAHIC Ext. BNL. Simulations: (A) pH 5.3; (B) pH 5.6; (C) pH 5.9; (D) pH 6.2. Solid blue lines: lowest scoring prediction; Solid brown lines: median scoring prediction; Solid green lines: best scoring prediction; Dotted black lines: experiment. Batch isotherm fits: (E) pH 5.25; (F) pH 6.0. Capto Adhere column simulations and batch isotherm fit using SMAHIC Ext. BFI. Simulations: (G) 5 CV gradient length; (H) 10 CV gradient length; (I) 20 CV gradient length; (J) 30 CV gradient length. Batch isotherm fit: (K) pH 8.0. Note that the isotherm fits correspond to the best column predictions.

and overfitting to the batch data. In any case, these results further support the finding that additional parameters were not required to describe the contributions of hydrophobic interactions when this can be readily accomplished with the K_s parameter. Interestingly, for SMAHIC, the removal of K_s and K_p resulted in a significant reduction in the quality of the predictions (shown in the supplementary material Excel datasheet), indicating that the elution behavior resulting from the U-shaped isotherm could not be accurately predicted without the use of the K_s parameter.

4.8. Analysis of model performance using scoring metrics

Although a qualitative comparison of the experimental and simulated profiles informs model performance, a quantitative approach paves a clearer road towards model qualification. To this end, statistical analyses were performed by calculating scores for both the Capto MMC column predictions and batch data fits. Column prediction scores were calculated using a weighted sum of NRMSE and peak shape deviation (first moment ΔFM, peak width ΔPW, and peak maxima ΔPM) as described in Section 3.11. Batch isotherm scores were calculated solely from the NRMSE of the fits. Scores were calculated for all models and repeats, using both BFI and BNL data. Fig. 7 shows the distribution of column (Fig. 7A, 7C) and batch (Fig. 7B, 7D) scores for all models using BFI and BNL data, respectively, visualized using boxplots. All twenty repeated fits and simulations are visualized, where the box minima and maxima represent the worst and best repeats, respectively. Further, the box borders represent the lower

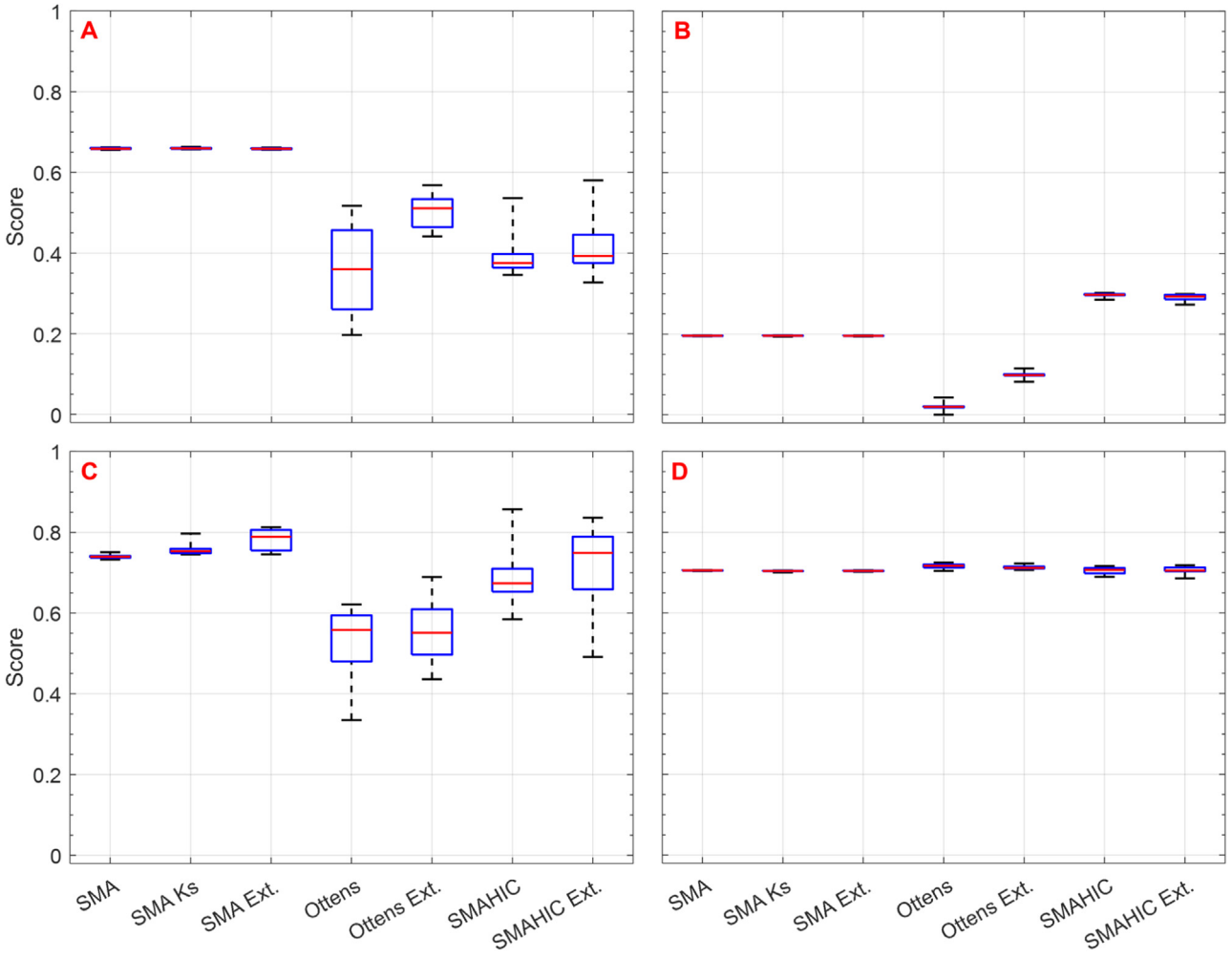

Fig. 7. Boxplots of Capto MMC BFI and BNL score distributions. BFI scores: (A) column predictions; (B) batch isotherm fits. BNL scores: (C) column predictions; (D) batch isotherm fits.

and upper quartiles with the box centerline representing the median.

Overall, BNL is superior to BFI, for this data set, due to the BNL score distributions being consistently higher for both column and batch. This result for the batch fits is unsurprising, since the reduced number of data points leads to improved fits to the data. However, the result for the column predictions illustrates that the presence of low protein concentration data points universally skews the model performance for this data set. While the trends in scores for BFI and BNL share some similarities, there are notable differences, particularly for the batch scores. For BFI, SMA and its two variants are the highest scoring models and achieve equal scores with seemingly no variability between repeats. For BNL, the highest median score was seen for the SMA Ext. model, followed by the other SMA-type models. While the SMAHIC model achieved the highest score on a single repeat, this result was an outlier (3 standard deviations above the median score). Both BFI and BNL column scores show that there is a clear relationship between variability and model complexity (i.e., number of isotherm parameters). This relationship is expected, due to the increasing uncertainty in parameter estimation that accompanies larger optimization problems. Interestingly, while significant differences in variability are seen in the column scores, minor differences were seen in the batch scores, strongly suggesting that the quality of the batch data fit is not an adequate determinant of the quality of column predictions. Although the column scores mildly trended with batch scores for BFI, no such trends are seen for BNL. The discrepancy is so prominent for BNL that there is no discernible difference between batch scores for any of the models, while the column scores were seen to vary substantially. One possible explanation for this finding is that the data is overfit for the complex isotherm models and leads to some poorly determined isotherm parameters. More specifically, due to the considerable number of parameters being fit, relative to the minimal number of data points, excellent fits can be achieved using each model—however with high variability in the estimated isotherm parameters.

One noteworthy trend within the BNL column prediction score distribution (Fig. 7C) is between SMA, SMA K_s, and SMA Ext. The median column prediction scores increase with both modifications, which is consistent with the clear improvement in the qualitative comparisons shown in the chromatograms. As expected, this enhancement is accompanied by an increase in variability. Even so, the lowest column scores for the modified SMA models are no worse than the best score for the unmodified SMA, indicating that the modified models are at least as well-performing as SMA. This is not the case, however, for the Ottens models, which seem to have both a notable increase in variability as well as an overall decrease in column score. In addition, the SMAHIC and SMAHIC Ext. models appear to have some repeats that can contend with

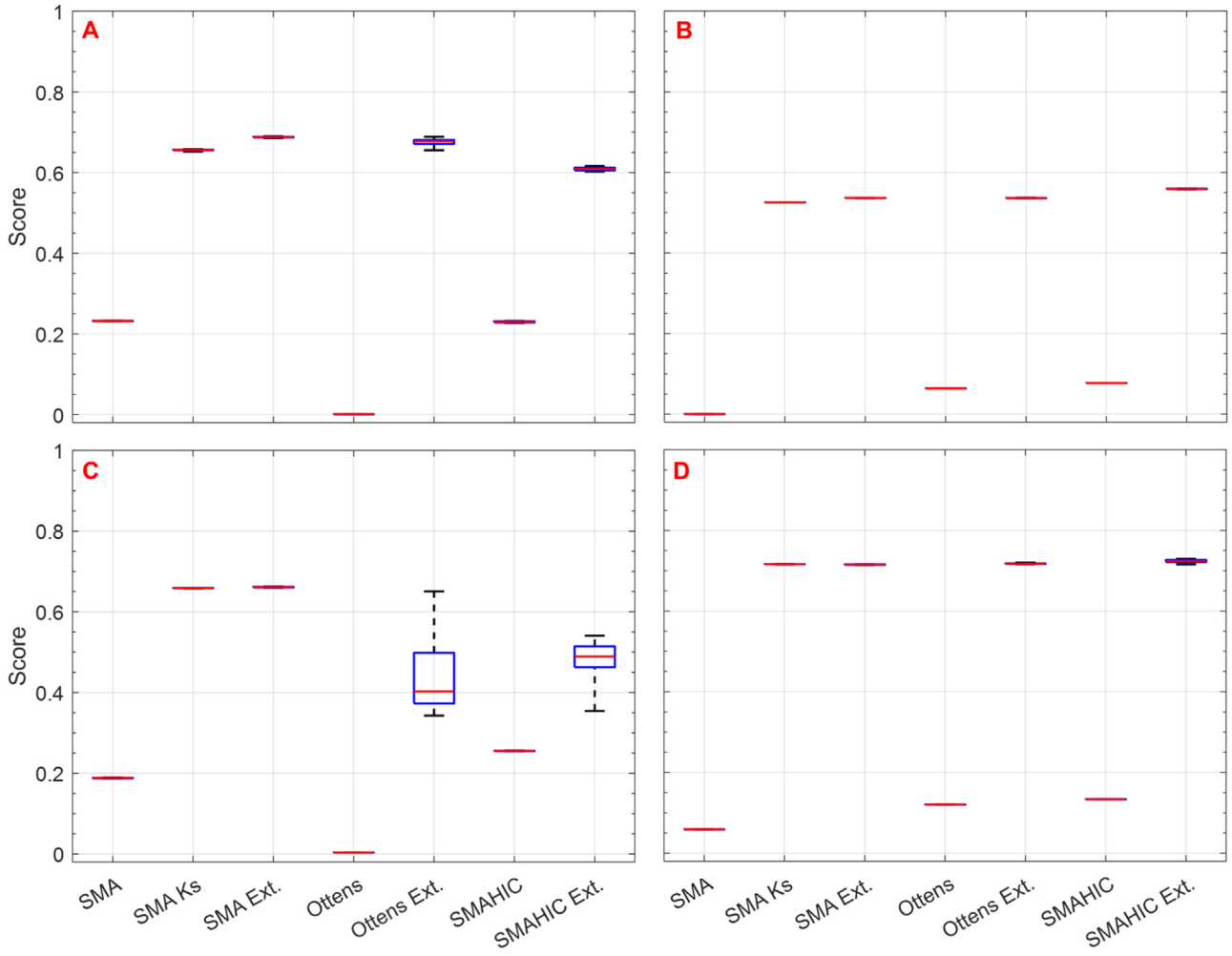

Fig. 8. Boxplots of Capto Adhere BFI and BNL score distributions. BFI scores: (A) column predictions; (B) batch isotherm fits. BNL scores: (C) column predictions; (D) batch isotherm fits.

the SMA models; however, their extreme inconsistency between repeats makes them undesirable. Overall, it appears that the set of SMA models are the highest performing out of all the models studied in this work.

Employing the same methodology for Capto Adhere, score distributions are visualized in Fig. 8, where Fig. 8A and 8B correspond to the column predictions and isotherm fits for BFI, respectively, and Fig. 8C and 8D correspond to those for BNL. Unlike the findings shown for Capto MMC, here the scores for column and batch clearly trend with each other. This is because the isotherm must be able to capture the U-shaped binding trend in order to be able to predict the shrinking peak with increasing gradient slope in the MMAEX system. As shown by the score distributions, the only models that achieve a reasonable score are SMA K_s, SMA Ext., Ottens Ext., and SMAHIC Ext. The commonality between these models is the inclusion of the K_s parameter—the models that do not have this parameter (SMA, Ottens and SMAHIC) fail to achieve reasonable scores for both isotherm fits and column predictions. While all four isotherms that included the K_s term performed similarly with the batch data, there was a clear difference for the column simulations. As can be seen, both modified SMA models achieved predictions of equal or better quality as compared to Ottens Ext. and SMAHIC Ext. predictions with smaller variation between repeats, despite not having parameters explicitly describing the stoichiometry of hydrophobic interactions.

It is interesting to note that the score distributions for BNL (Fig. 8C and 8D) were similar to that of BFI (Fig. 8A and 8B). This is in sharp contrast to the results for Capto MMC where models based on the BFI and BNL data resulted in quite different behavior where BNL significantly outperformed BFI for all models in the MMC system. One of the reasons for this might be that while the isotherm shapes for Capto MMC were extremely favorable (square), the initial slopes for Capto Adhere had a shallow uptake which resulted in the low concentration region being significantly less error prone.

Importantly, the score distributions showed that the SMA Ext. isotherm was the best performing model (i.e., highest median score) for both multimodal resins. This key finding indicates that the terms accounting for explicit (stoichiometric) hydrophobic contributions were not only unneeded in the model formulation, but also detrimental to overall model performance. Notwithstanding, the inclusion of these parameters was less problematic for Capto Adhere compared to Capto MMC—the relative changes in score median and spread were less noticeable. Implied in this finding is the impact of model complexity (number of isotherm parameters), which poses a disadvantage to the explicit multimodal isotherm formalisms—particularly in terms of prediction variability. To better understand this impact, further analysis was conducted to better incorporate the impact of prediction variability on selection criteria.

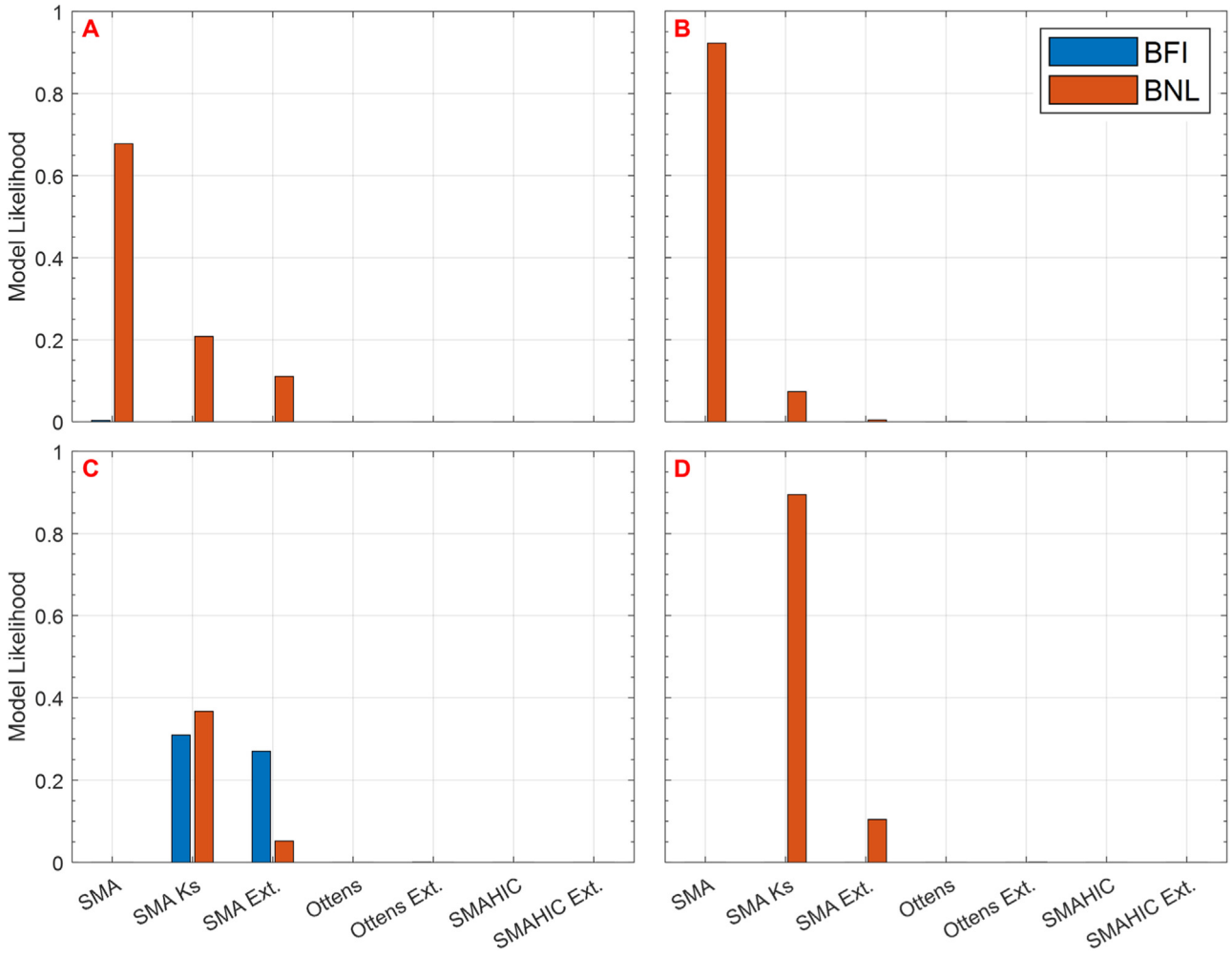

Fig. 9. Model likelihood histograms calculated from AIC scores for BFI (blue) and BNL (orange). Capto MMC histograms: (A) column predictions; (B) batch isotherm fits. Capto Adhere histograms: (C) column predictions; (D) batch isotherm fits.

4.9. Application of Akaike information criterion

The Akaike information criterion (AIC) was employed to further aid in model discrimination. AIC analysis is a method that facilitates model differentiation via a scoring system that ranks individual models within a considered set. The criterion contrasts the benefits of prediction accuracy through a log likelihood term and the drawbacks of model complexity based on the number of parameters. AIC is similar to the Bayesian information criterion (BIC)—only differing in the formulation of the penalty term. Models are ranked with respect to their likelihoods (i.e., probability of being selected) to help facilitate their selection. In practice, the selection process is not as simple as choosing the model with the highest likelihood; rather, this metric can be used to inform the user on the benefits of model performance versus its complexity. Further, increased model complexity may be linked with inconsistency in performance, particularly when the model parameters are fitted and are predisposed to higher variability (proportional to the scale of the optimization problem). While the AIC does not directly inform the influence of added model parameters, it does suggest that when parameters are added to an existing model in the set, there must be a benefit associated with their addition for likelihood to increase—or at the very least, to not decrease substantially.

Here, AIC was calculated from the residual of the scores for both column predictions and batch fits. AIC values were translated into model likelihoods as described in Section 3.11. Fig. 9 shows the distribution of BFI and BNL model likelihood values for both resins using the whole series of isotherm models with respect to column predictions (Fig. 9A and 9C, for Capto MMC and Capto Adhere, respectively) and batch fits (Fig. 9B and 9D, for Capto MMC and Capto Adhere, respectively). The results for Capto MMC indicated that there was clearly a drastic preference given towards BNL compared to BFI, since the likelihoods for BFI were extremely low, with only SMA BFI having a nonzero probability. This aspect of the distribution confirmed the prior observation that BNL is superior to BFI for the Capto MMC data set. As for model selection within the BNL distribution, both the column and batch analysis suggest that the only models worth considering, for this data set, are SMA, SMA K_s and SMA Ext.—implying that there is no justification for selecting any of the more complex multimodal isotherms. This finding for the batch scores is unsurprising, since there was no difference in the fits between the models and the AIC score negatively weights their complexity. Model likelihoods for the column predictions thus have a greater bearing on the ultimate model selection. While the SMA model shows the highest likelihood of being selected, this does not necessarily imply that the modified SMA models should not be considered. The probabilities here are simply suggestions based on the relative merits and complexities of each model and are intended to narrow down the considered set of models. The accuracy of column predictions for SMA K_s and SMA Ext. both appeared to improve (qualitatively) with respect to the accuracy of the base SMA model. However, this improvement

was accompanied by a decrease in model consistency (i.e., variability between repeats), indicating that there is an apparent influence of model complexity on robustness. Since the AIC scores include the score for all repeats in the analysis, this relationship is accounted for, along with the penalty associated with having more parameters. As a result, the SMA model is suggested by the AIC as the best option, due to the decreased consistency of the modified SMA models. This result highlights the importance of considering both visual as well as statistical measures for model differentiation. Overall, the SMA Ext. model is arguably the most suitable isotherm formalism for modeling the Capto MMC system in this study.

Employing the AIC for the Capto Adhere column predictions and batch fits (Fig. 9C and 9D) showed that only the modified SMA models were recommended because they achieved comparable scores to the more complex multimodal models, while having fewer parameters. This finding confirms that for both Capto MMC and Capto Adhere, under the conditions studied, the modified SMA models outperformed the more complex multimodal isotherms by achieving predictions of equal or greater quality while containing fewer parameters. The AIC results for Capto Adhere also indicate that comparable model likelihoods were achieved for the modified SMA models when BFI or BNL data sets were used for the column predictions. On the other hand, for the isotherm fits, BNL was suggested—which is not surprising since the fits are expected to improve when fewer data points are included. It is worth noting that BNL has the added benefit of requiring less data, effectively reducing the experimental burden, which implies that it should be selected here. From a qualitative and quantitative standpoint, the SMA K_s is the best isotherm for modeling the of unique behavior of Capto Adhere in this study.

4.10. Sensitivity analyses for isotherm parameters

Having shown that the SMA model and its modified counterparts are the most appropriate models to consider for the Capto MMC dataset, further analysis was performed to shed some light on the relative contributions of the isotherm parameters on the model outputs. As described in Section 3.12, first-order sensitivity analyses were performed for the BNL models using the elementary effects method, also called one-at-a-time (OAT) analysis. Briefly, the method involves an iterative process where a parameter is changed by a fixed percentage (perturbation), a simulation is performed, and the variance is calculated using a differential between the native simulation (unmodified parameter) and the new simulation (modified parameter). This process is repeated for all perturbation values, all models, and all model parameters. Here, the method was employed to determine the impact of each isotherm parameter on both column predictions and batch fits, using twenty perturbation values (0.1 to 2% in 0.1% steps) for a wholistic depiction of sensitivities. Once the variances are calculated, sensitivity scores for each parameter can be determined by essentially normalizing relative variance with respect to total variance (for all models). The resulting sensitivity scores represent the relative influence that each parameter has on the output of the function—with greater score indicating a greater importance. As such, the sum of scores for a single model sum to unity. By comparing the scores for isotherm parameters that are shared between models, the overall importance of certain parameters in the model frameworks can be ascertained. This method is ideal for determining parameter contributions within computationally expensive models as compared to variance-based methods which require significantly more function evaluations (simulations).

It is important to note the limitations of this method—it is applicable towards understanding first-order sensitivities (individual parameters) and not higher-order sensitivities (groups of parameters). Thus, this analysis cannot be used to describe the interactions between parameters that may occur—especially when using models with many parameters. The benefit of OAT analysis is that it can be performed with a reduced number of simulations (order of hundreds [84]), while higher-order sensitivity analysis, such as variance-based methods, require many simulations (order of thousands or tens of thousands) and are typically performed using a Monte Carlo configuration [85] instead of one-at-a-time sampling.

Comparing the trends in Capto MMC BNL parameter sensitivity between the column predictions (Fig. 10A) and batch fits (Fig. 10B) yields notable differences. While $K_{eq,1}$ had the highest sensitivity for most of the models using column simulations, it was not important for the batch fits, where σ was shown to be the most influential. It is plausible that σ would be more impactful in fitting the batch data because this parameter is directly related to the saturation capacity, which is reached during the batch experiments but not in the column experiments. The remaining parameters that had a discernible impact for batch were ν_0 and $K_{eq,0}$; these parameters also affected the column results, although to a greater degree (i.e., higher sensitivity compared to batch). Further analysis of the sensitivity trends also indicated that the particularly important isotherm parameters tended to be those that are present in mathematically impactful regions of the functional form, assuming that their magnitude was not minute. For example, ν_0 had high sensitivity in most models and is present in two exponential terms in all isotherm models. On the other hand, ν_1 has low values of sensitivity which can be expected because it has such small values. Since the perturbations are used as fixed percentages of each parameter, those with near zero values would tend to affect the outputs (column simulation or batch fits) minimally.

Another cause of sensitivity differences for Capto MMC is the influence of other input parameters that change over the course of the simulation (e.g., pH, ionic strength, and protein concentration). One example of this is the difference in sensitivities between $K_{eq,1}$, K_s, and K_p, which are all present within exponential terms. Sensitivities for these parameters would naturally be affected by the magnitude of the concentration terms that they are multiplied by (pH, ionic strength, and protein concentration). Interactions between parameters can also affect their individual sensitivities. For instance, $K_{eq,0}$ is not present in an exponential term, but is multiplied by these parameters that are potentially affecting its sensitivity. Further, n_0 is unimpactful for Ottens Ext. but becomes important for SMAHIC Ext. once β_0 is included in the formulation. Since these terms are multiplicative, it is reasonable to think that they would have some influence on each other. The included salt dependence of β adds another dimension to this interaction, because n does not have ties to the salt concentration. While these examples help elucidate the inner workings of these isotherm formalisms, higher-order sensitivity analyses would provide a more detailed understanding and are a worthy consideration for future investigation.

To better understand the contributions of the isotherm parameters for Capto Adhere, the same approach of sensitivity analysis was carried out, using only the BFI data. First-order sensitivity analyses were again performed for each model and each isotherm parameter, shown in Fig. 10C for column predictions and Fig. 10D for batch fits. Here, the only models shown are those containing K_s, since the remaining models had extremely poor prediction scores for Capto Adhere. For the sensitivity in column predictions, the most impactful parameters were K_s, ν, and σ with K_s having the highest impact for the majority of the models shown. In contrast, for the batch fits ν had the greatest impact. One explanation for the importance of ν in the batch fits may be its impact on the initial slope of the adsorption isotherm which may be less important in the column simulations. Importantly, all the parameters explicitly describing hydrophobic interaction stoichiometry were less influential. This further highlights the importance of the K_s pa-

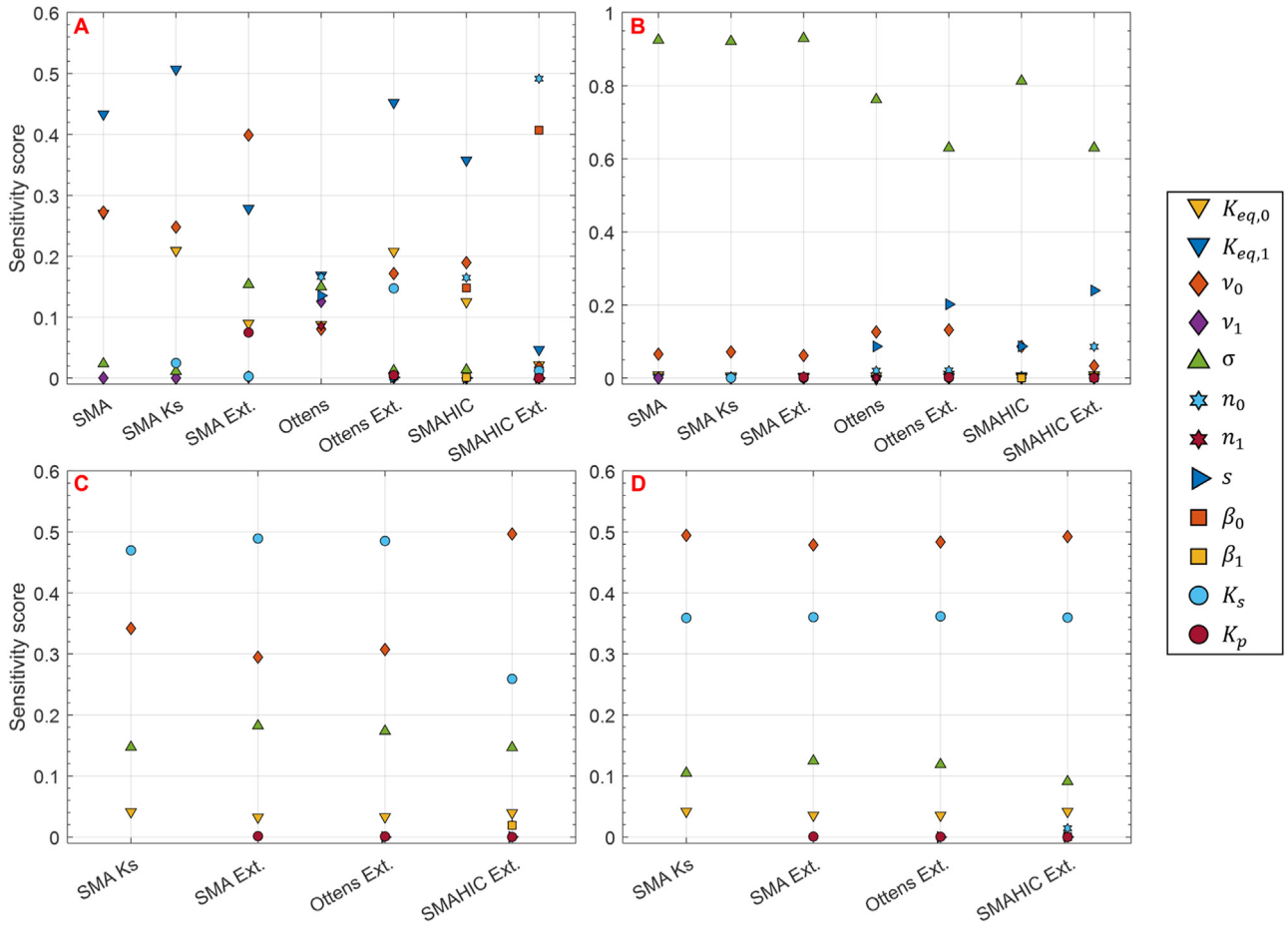

Fig. 10. Scatter plot of first-order sensitivity scores for each isotherm parameter in each model. Capto MMC BNL sensitivities: (A) column predictions; (B) batch isotherm fits. Capto Adhere BFI sensitivities: (C) column predictions; (D) batch isotherm fits. Note the differences in axes and that parameter symbols not visible for a given model are either not present in the formulation or are visually overlapping with another parameter symbol.

rameter for being able to capture the hydrophobic nature of the system and unique elution behavior stemming from the U-shaped isotherm.

4.11. Parametric study for K_s parameter

To better understand the dependence of isotherm shape and elution behavior on K_s, a parametric study was performed to study U-shape isotherm binding trends (retention factor k' vs. salt concentration), elution peak shape, and elution recovery with respect to changing K_s for the SMA K_s model. To this end, k' was calculated at discrete values of K_s between 0 M^{-1} and 14 M^{-1} in steps of 1 M^{-1} using Eq. (31),

$$k' = \varphi\left(\lim_{c\to 0}\frac{q_p}{c_p}\right) = \varphi K_{eq}\exp(K_s c_s)\left(\frac{\Lambda}{c_s}\right)^{\nu} \tag{31}$$

which can be derived from the definition of the retention factor [54] and the equilibrium form of the SMA K_s isotherm, where the phase ratio $\varphi = (1-\varepsilon_t)/\varepsilon_t$. In this analysis, while K_s was changed, the remaining isotherm parameters in the Capto Adhere SMA K_s BFI model were held constant as those used in Fig. 3. Fig. 11 shows the relationship between $\ln k'$ and salt concentration c_s with respect to changing K_s. At K_s of zero (SMA model), there is a clearly a monotonic trend in binding affinity with respect to salt concentration, which is expected for the SMA model. As the value of K_s increases, the left side (zero salt) remains unchanged; however, the right side (high salt) continually increases. Since binding affinity grows exponentially with salt concentration according to the

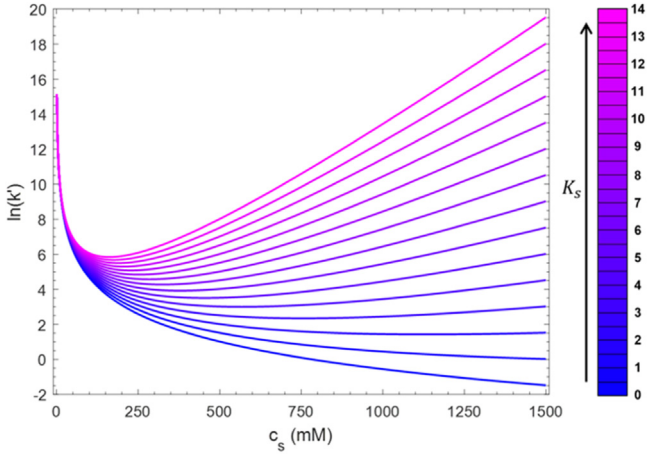

Fig. 11. Parametric plots showing the effect of K_s parameter on linear binding trends (ln(k') vs. salt concentration). Capto Adhere SMA K_s BFI model is used with all parameters held constant except for K_s, which is varied.

value of K_s, the relative influence of this parameter changes with salt concentration. At intermediate values of K_s, a U-shaped binding trend begins to form. Since the expected reason for the existence of the U-shape here is a transition to a hydrophobic interaction dominated regime, K_s is capable of capturing the effect of hydrophobic interactions. Thus, by changing K_s alone, the modified

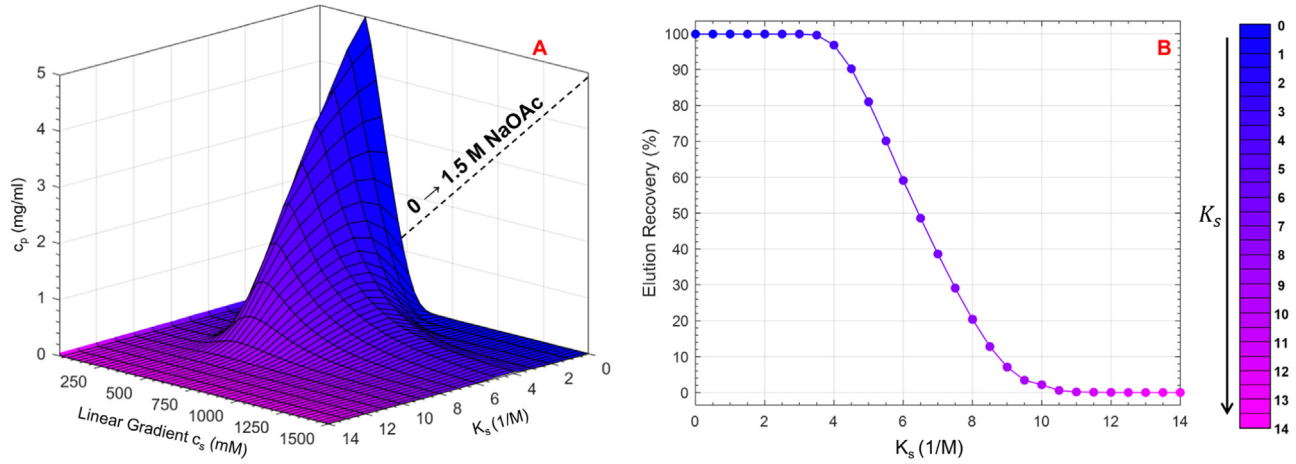

Fig. 12. Parametric plots showing the effect of K_s parameter on LGE peak shape (A), dotted black line showing the linear NaOAc gradient, and elution recovery (B). Capto Adhere SMA K_s BFI model is used with all parameters held constant except for K_s which is varied.

SMA model can be used to capture the effect of hydrophobic interactions at moderate to high salt concentrations. This capability illustrates the utility of the SMA K_s model to capture a complex set of interactions while containing a minimized set of model parameters.

Expanding on the utility of the K_s parameter, linear gradient simulations, shown in Fig. 12A, were performed from 0 to 1.5 M NaOAc in 30 CV at values of K_s ranging from 0 to 14 M^{-1} with calculated elution recoveries shown in Fig. 12B. As an implication of the U-shape isotherm behavior, a loss in protein recovery evidently occurs at values of K_s greater than 4 M^{-1} for this set of isotherm parameters. This trend continues until K_s of 12 M^{-1} where the elution peak completely disappears, and no protein recovery is obtained. This effect can be explained by the exponential effect of K_s resulting in significant growth of binding affinity and capacity with respect to increasing salt concentration. Thus, it is clear that K_s can be employed effectively as a means to model peak shape and recovery loss in both MMCEX and MMAEX systems.

4.12. Advantages and limitations

In addition to providing insight on isotherm selection, the workflow and methods utilized in this work also provide a framework for accurate prediction of column elution behavior using batch isotherm data. A key advantage of this approach is the accelerated timeline required for model development, in reference to models based on column elution or breakthrough experiments. The high-throughput nature of the batch experiments allows isotherms over a full set of loading, salt, and pH conditions to be developed in the span of a few hours. Further, limiting the required loading conditions to the nonlinear region of the isotherm (BNL) further reduces the experimental burden. In this study, the Capto MMC batch isotherm experiment was completed in under two hours with the full set of isotherm data developed using only two 96-well plates. In contrast, column linear elution experiments, typically used for model construction, span roughly 1–2 h each with roughly ten experiments required to span an identical range of pH [58]. For example, four sets of three linear gradient experiments performed at different slopes, each set at a different pH, would result in twelve experiments for four pH conditions (12–24 h total). With stringent timelines common in early-stage process development, expedient model development workflows are crucial, suggesting that batch isotherm experiments would be prudent to employ. Further, the computational expense of fitting batch isotherm data is significantly lower than the cost of inverse fitting of column data because the equilibrium equations are algebraic in nature which are much easier (computationally) to solve compared to column simulations.

A limitation of the current workflow presented in this study is that obtaining high quality fits to batch isotherm data do not guarantee accurate elution predictions; thus, it is difficult to identify an appropriate isotherm formalism without having protein elution data to validate the model. Accordingly, the authors recommend that a small set of elution experiments be performed in addition to batch isotherm generation so that the model parameters can be validated with confidence. It is also prudent to perform multiple fits to the batch data so that variability in parameter fitting (due non-deterministic global optimization schemes) does not negatively affect the quality of the generated regressed isotherm parameters.

While the modified SMA model was shown to be extremely useful for modeling elution behavior on Capto MMC, one could envision scenarios where more hydrophobic MMCEX ligands could result in more complex adsorption behavior which may impact the utility of this isotherm as compared to the more complex isotherm formalisms. However, since Capto MMC is one of the more hydrophobic MMCEX ligands that are commercially available, it is likely that the modified SMA model will perform well with many of the commercially available resins at typical pHs of operation. For cases when pH is particularly low (e.g., near the pKa of the weakly charged multimodal ligand—4.64 for Capto MMC [68]), the relative contribution of hydrophobic interactions is expected to be greater in comparison to electrostatic interactions. While the complex multimodal isotherms may be more appropriate here, it is reasonable to expect that the extended SMA model could still work well because the K_s parameter was demonstrated, in the parametric study, to precisely account for hydrophobic interactions.

The focus with Capto Adhere in this study was centered around modeling of unique elution patterns on Capto Adhere caused by non-monotonic binding affinity trends. While this behavior was intriguing, the conditions studied were limited to one pH condition. It has been shown by Lee et al. [16] that in MMAEX the U-shape trend at high pH can transition to a monotonically increasing binding with salt at low pH. As shown in the current work, U-shape behavior was seen at pH values near the pI of the mAb. It follows that a transition from purely HIC-like behavior to U-shape behavior (i.e., increased binding at low ionic strength) must occur in this scenario as pH increases. It follows that accounting for this transition will require pH to be included in the model formulation.

Expanding on this work by accounting for pH in the MMAEX system would open up useful avenues for model-based process development. One example of this is weak-partitioning chromatography (WPC)—a variant of flow-through mode where the eluent conditions (pH and ionic strength) are modulated to optimize the resin's capacity for the impurity at the cost of some product loss to adsorption. This process with AEX or MMAEX is typically performed at a pH below the pI, where pH and ionic strength are varied to control the differential binding affinity between the product and impurity in the flow-through mode [86]. Processes such as WPC in multimodal systems can be modeled flexibly by including both pH and ionic strength in the model formulation.

Identification of mechanistic models that can bridge these gaps would greatly benefit the community and improve the understanding of multimodal chromatography. Another natural extension of this work would be to broaden the set of considered proteins, resins, and mobile phase conditions. To this end, future work in this space should extend the model identification efforts to include proteins with a diverse range of biophysical properties (particularly surface charge and hydrophobicity), ligands with a broader set of chemistries, and wider sets of mobile phase conditions (e.g., salt, pH, and additional modifiers).

5. Conclusions

Although column modeling has been extensively studied for single-mode chromatographic systems such as IEC and HIC, it has been explored to a much lesser extent for multimodal resins. The primary reason for this discrepancy is, arguably, the lack of agreement of which isotherm model to employ for multimodal chromatography. In this study, we have sought to address this issue by exploring an array of isotherm formalisms and characterizing them based on their predictive abilities and relative complexities. The set of isotherm models studied were all based on the stoichiometric displacement framework, with considerations for electrostatic interactions, hydrophobic interactions, and thermodynamic activities. Isotherm parameters for each model were robustly determined through twenty repeated fits to a set of mAb – Capto MMC batch isotherm data spanning a wide range of loading, ionic strength, and pH as well as a set of mAb – Capto Adhere batch data. The batch isotherm data were used in two varieties, covering the full range of loading (batch full isotherm—BFI), and containing only the high concentration data points (batch no linear—BNL). Predictive ability was characterized by the model's capacity to capture notable changes in salt gradient elution behavior with respect to pH for Capto MMC and to capture unique elution patterns with respect to gradient slope for Capto Adhere. For both resins, model performance was measured using a scoring metric based on agreement in peak characteristics. Model complexity was also considered through use of the Akaike information criterion (AIC), which incorporated the score distributions as well as a negative penalty based on the number of model parameters.

While the same approach was employed for both resins, key differences were found in the way the models should be employed for each resin. More specifically, for the MMCEX system, model performance benefitted substantially from removal of low protein concentration data (corresponding to the linear region of the isotherm). This was not the case for the MMAEX system, where removal of the low protein concentration batch data did not improve predictions—likely due to the qualitatively different shapes of the isotherms. Beyond the impact of loading conditions, key similarities were found in the top-performing isotherm models for both resins. Comparison of Capto MMC scores between models showed that the extended SMA model (SMA with two activity coefficient terms) had the highest median score for the twenty column simulations performed using each set of isotherm parameters. Analysis of the AIC model likelihoods (i.e., the probability that the model should be selected) showed that the SMA model and its two modified variants were the only models worth considering. Consideration of model performance from both a qualitative (visual agreement with experimental column elution curves) and quantitative standpoint lead to the conclusion that the extended SMA isotherm, containing two modifications K_s and K_p (tied to an exponential dependence on salt and protein concentration, respectively), was the top contender for modeling of the MMCEX system. Additionally, the more complex isotherm models that explicitly accounted for hydrophobic interaction stoichiometry showed no benefit over the SMA models for this application.

As for Capto Adhere, the SMA K_s isotherm (containing K_s but not K_p) obtained highly accurate column predictions and fits to the batch data. The predictions obtained with isotherm models explicitly accounting for both electrostatic and hydrophobic interactions did not, like the MMCEX system, outperform the modified SMA model, thereby suggesting that there was no added benefit of the additional isotherm parameters. This finding was confirmed with the scoring metric and the Akaike information criterion, which suggested that the modified SMA model should be selected due to it having fewer parameters. Further, sensitivity analyses performed for each isotherm parameter in each formalism illustrated that the K_s parameter had a significant impact on both column predictions and batch fits. To provide further insight on this finding, a parametric study was conducted to illustrate the influence of K_s on binding affinity and elution behavior. This investigation showed that K_s provides facile control of U-shaped retention curves and elution peak shape. Overall, the efforts in this study led to identification of simplified isotherm formalisms capable of accurately predicting a wide range of column behavior for both a multimodal cation-exchange and multimodal anion-exchange resin.

Declaration of Competing Interest

The authors declare the following financial interests/personal relationships which may be considered as potential competing interests.

Steven Cramer reports financial support was provided by National Institute for Innovation in Manufacturing Biopharmaceuticals.

CRediT authorship contribution statement

Scott H. Altern: Conceptualization, Data curation, Formal analysis, Investigation, Methodology, Validation, Visualization, Writing – original draft. **John P. Welsh:** Conceptualization, Methodology, Resources. **Jessica Y. Lyall:** Conceptualization, Methodology, Resources. **Andrew J. Kocot:** Investigation. **Sean Burgess:** Conceptualization. **Vijesh Kumar:** Conceptualization. **Chris Williams:** Conceptualization, Supervision, Resources. **Abraham M. Lenhoff:** Conceptualization, Supervision, Resources. **Steven M. Cramer:** Conceptualization, Investigation, Writing – review & editing, Supervision, Funding acquisition.

Data availability

The authors are unable to share the data for batch isotherms and column elution profiles; however, the isotherm parameters are included in the supplementary material and the code (IsoFit) is available at https://github.com/alters9595/IsoFit.

Acknowledgements

This work was performed under a Project Award Agreement from the National Institute of Innovation in Manufactur-

ing Biopharmaceuticals (NIIMBL) and financial assistance award 70NANB17H002 from the U.S. Department of Commerce, National Institute of Standards and Technology. We are grateful to Tobias Hahn at GoSilico/Cytiva for providing a license to the ChromX software and for his continued technical support. We are also grateful to Jamie Peyser at Repligen for providing the prepacked columns used in this work. Further, we are grateful to Abraham Lenhoff and Matthew Armstrong at the University of Delaware for providing the code for the parallel tempering optimization algorithm. We are also grateful for the support of Elnaz Rasti Boroujeni and Nicole Lee-Nguyen at Genentech for performing the Capto MMC batch experiments as well as the support of Joe Boerma and Michael Rauscher at Merck for performing the Capto Adhere batch experiments. Additionally, we are grateful to David Roush at Merck for reviewing the manuscript and to Angela Moser at RPI for proofreading. Lastly, we are grateful to Jake Klockowski, who assisted with construction of the isotherm fitting routines.

Supplementary materials

Supplementary material associated with this article can be found, in the online version, at doi:10.1016/j.chroma.2023.463878.

References

[1] J. Chen, J. Tetrault, Y. Zhang, A. Wasserman, G. Conley, M. DiLeo, et al., The distinctive separation attributes of mixed-mode resins and their application in monoclonal antibody downstream purification process, J. Chromatogr. A 1217 (2010) 216–224, doi:10.1016/j.chroma.2009.09.047.

[2] H.S. Karkov, B.O. Krogh, J. Woo, S. Parimal, H. Ahmadian, S.M. Cramer, Investigation of protein selectivity in multimodal chromatography using in silico designed Fab fragment variants, Biotechnol. Bioeng. 112 (2015) 2305–2315, doi:10.1002/bit.25642.

[3] J.A. Woo, H. Chen, M.A. Snyder, Y. Chai, R.G. Frost, S.M. Cramer, Defining the property space for chromatographic ligands from a homologous series of mixed-mode ligands, J. Chromatogr. A 1407 (2015) 58–68, doi:10.1016/j.chroma.2015.06.017.

[4] J. Woo, S. Parimal, M.R. Brown, R. Heden, S.M. Cramer, The effect of geometrical presentation of multimodal cation-exchange ligands on selective recognition of hydrophobic regions on protein surfaces, J. Chromatogr. A 1412 (2015) 33–42, doi:10.1016/j.chroma.2015.07.072.

[5] S.M. Timmick, N. Vecchiarello, C. Goodwine, L.E. Crowell, K.R. Love, J.C. Love, et al., An impurity characterization based approach for the rapid development of integrated downstream purification processes, Biotechnol. Bioeng. 115 (2018) 2048–2060, doi:10.1002/bit.26718.

[6] N. Kateja, D. Kumar, A. Godara, V. Kumar, A.S. Rathore, Integrated chromatographic platform for simultaneous separation of charge variants and aggregates from monoclonal antibody therapeutic products, Biotechnol. J. 12 (2017) 1–12, doi:10.1002/biot.201700133.

[7] K.A. Kaleas, C.H. Schmelzer, S.A. Pizarro, Industrial case study: evaluation of a mixed-mode resin for selective capture of a human growth factor recombinantly expressed in E. coli, J. Chromatogr. A 1217 (2010) 235–242, doi:10.1016/j.chroma.2009.07.023.

[8] C.L. Bilodeau, N.A. Vecchiarello, S. Altern, S.M. Cramer, Quantifying orthogonality and separability: a method for optimizing resin selection and design, J. Chromatogr. A 1628 (2020) 1–31, doi:10.1016/j.chroma.2020.461429.

[9] N. Vecchiarello, S.M. Timmick, S. Cramer, A framework for calculating orthogonal selectivities in multimodal systems directly from cell culture fluid, Biotechnol. Bioeng. 119 (2022) 299–314, doi:10.1002/bit.27977.

[10] L.A. Kennedy, W. Kopaciewicz, F.E. Regnier, Multimodal liquid chromatography columns for the separation of proteins in either the anion-exchange or hydrophobic-interaction mode, J. Chromatogr. A 359 (1986) 73–84, doi:10.1016/0021-9673(86)80063-2.

[11] D. Gao, D.Q. Lin, S.J. Yao, Patch controlled protein adsorption in mixed-mode chromatography with benzylamine as functional ligand, Biochem. Eng. J. 38 (2008) 355–361, doi:10.1016/j.bej.2007.07.024.

[12] B.K. Nfor, M. Noverraz, S. Chilamkurthi, P.D.E.M. Verhaert, L.A.M. van der Wielen, M. Ottens, High-throughput isotherm determination and thermodynamic modeling of protein adsorption on mixed mode adsorbents, J. Chromatogr. A 1217 (2010) 6829–6850, doi:10.1016/j.chroma.2010.07.069.

[13] R.B. Gudhka, D.J. Roush, S.M. Cramer, A thermodynamic evaluation of antibody-surface interactions in multimodal cation exchange chromatography, J. Chromatogr. A 1628 (2020), doi:10.1016/j.chroma.2020.461479.

[14] J. Pezzini, C. Cabanne, R. Gantier, V.N. Janakiraman, X. Santarelli, A comprehensive evaluation of mixed mode interactions of HEA and PPA HyperCel™ chromatographic media, J. Chromatogr. B Anal. Technol. Biomed. Life Sci. 976-977 (2015) 68–77, doi:10.1016/j.jchromb.2014.11.020.

[15] Parasnavis S. Insights into the purification of bispecific antibodies on multimodal systems: from chromatography to biophysics 2021.

[16] Y.F. Lee, H. Graalfs, C. Frech, Thermodynamic modeling of protein retention in mixed-mode chromatography: an extended model for isocratic and dual gradient elution chromatography, J. Chromatogr. A 1464 (2016) 87–101, doi:10.1016/j.chroma.2016.08.026.

[17] W.R. Melander, Z. El Rassi, C. Horváth, Interplay of hydrophobic and electrostatic interactions in biopolymer chromatography. Effect of salts on the retention of proteins, J. Chromatogr. A 469 (1989) 3–27, doi:10.1016/S0021-9673(01)96437-4.

[18] C. Machold, K. Deinhofer, R. Hahn, A. Jungbauer, Hydrophobic interaction chromatography of proteins: I. Comparison of selectivity, J. Chromatogr. A 972 (2002) 3–19, doi:10.1016/S0021-9673(02)01077-4.

[19] J.A. Roberts, G. Carta, Protein adsorption and separation with monomodal and multimodal anion exchange chromatography resins. Part I. Multicomponent adsorption properties and frontal chromatography, J. Chem. Technol. Biotechnol. (2022) 0–2, doi:10.1002/jctb.7239.

[20] A. Creasy, J. Lomino, G. Barker, A. Khetan, G. Carta, Gradient elution behavior of proteins in hydrophobic interaction chromatography with U-shaped retention factor curves, J. Chromatogr. A 1547 (2018) 53–61, doi:10.1016/j.chroma.2018.03.012.

[21] A. Creasy, J. Lomino, G. Carta, Gradient elution behavior of proteins in hydrophobic interaction chromatography with a U-shaped retention factor curve under overloaded conditions, J. Chromatogr. A 1578 (2018) 28–34, doi:10.1016/j.chroma.2018.10.003.

[22] C.L. Bilodeau, N.A. Vecchiarello, S. Altern, S.M Cramer, Quantifying orthogonality and separability: a method for optimizing resin selection and design, J. Chromatogr. A 1628 (2020), doi:10.1016/j.chroma.2020.461429.

[23] N. Vecchiarello, S.M. Timmick, C. Goodwine, L.E. Crowell, K.R. Love, J.C. Love, et al., A combined screening and in silico strategy for the rapid design of integrated downstream processes for process and product-related impurity removal, Biotechnol. Bioeng. 116 (2019) 2178–2190, doi:10.1002/bit.27018.

[24] S. Koley, S.H. Altern, M. Vats, X. Han, D. Jang, M.A. Snyder, et al., Evaluation of guanidine-based multimodal anion exchangers for protein selectivity and orthogonality, J. Chromatogr. A 1653 (2021) 462398, doi:10.1016/j.chroma.2021.462398.

[25] J.A. Roberts, G. Carta, Protein adsorption and separation with monomodal and multimodal anion exchange chromatography resins. Part II . Mechanisms of protein aggregation on the chromatographic surface, J. Chem. Technol. Biotechnol. (2022), doi:10.1002/jctb.7247.

[26] L. Zhang, S. Parasnavis, Z. Li, J. Chen, S. Cramer, Mechanistic modeling based process development for monoclonal antibody monomer-aggregate separations in multimodal cation exchange chromatography, J. Chromatogr. A 1602 (2019) 317–325, doi:10.1016/j.chroma.2019.05.056.

[27] J. Robinson, D. Roush, S.M. Cramer, The effect of pH on antibody retention in multimodal cation exchange chromatographic systems, J. Chromatogr. A 1617 (2020) 460838, doi:10.1016/j.chroma.2019.460838.

[28] K. Kallberg, H.O. Johansson, L. Bulow, Multimodal chromatography: an efficient tool in downstream processing of proteins, Biotechnol. J. 7 (2012) 1485–1495, doi:10.1002/biot.201200074.

[29] G. Zhao, X.Y. Dong, Y. Sun, Ligands for mixed-mode protein chromatography: principles, characteristics and design, J. Biotechnol. 144 (2009) 3–11, doi:10.1016/j.jbiotec.2009.04.009.

[30] B.K. Nfor, D.S. Zuluaga, P.J.T. Verheijen, P.D.E.M. Verhaert, L.A.M. Van der Wielen, M. Ottens, Model-based rational strategy for chromatographic resin selection, Biotechnol. Prog. 27 (2011) 1629–1643, doi:10.1002/btpr.691.

[31] H.G. Bock, D.H. Cebulla, C. Kirches, A. Potschka, Mixed-integer optimal control for multimodal chromatography, Comput. Chem. Eng. 153 (2021), doi:10.1016/j.compchemeng.2021.107435.

[32] V. Kumar, A.M. Lenhoff, Mechanistic modeling of preparative column chromatography for biotherapeutics, Annu. Rev. Chem. Biomol. Eng. 11 (2020) 235–255, doi:10.1146/annurev-chembioeng-102419-125430.

[33] C.A. Brooks, S.M. Cramer, Steric mass-action ion exchange: displacement profiles and induced salt gradients, AIChE J. 38 (1992) 1969–1978.

[34] W.R. Keller, M. Wendeler, Using multimodal chromatography for post-conjugation antibody-drug conjugate purification: a methodology from high throughput screening to in-silico process development, J. Chromatogr. A 1653 (2021) 462378, doi:10.1016/j.chroma.2021.462378.

[35] S.M. Pirrung, D. Parruca da Cruz, A.T. Hanke, C. Berends, R.F.W.C. Van Beckhoven, M.H.M. Eppink, et al., Chromatographic parameter determination for complex biological feedstocks, Biotechnol. Prog.. 34 (2018) 1006–1018, doi:10.1002/btpr.2642.

[36] H.S. Karkov, L. Sejergaard, S.M. Cramer, Methods development in multimodal chromatography with mobile phase modifiers using the steric mass action model, J. Chromatogr. A 1318 (2013) 149–155, doi:10.1016/j.chroma.2013.10.004.

[37] L. Sejergaard, H.S. Karkov, J.K. Krarup, A.B.B. Hagel, S.M. Cramer, Model-based process development for the purification of a modified human growth hormone using multimodal chromatography, Biotechnol. Prog. 30 (2014) 1057–1064, doi:10.1002/btpr.1923.

[38] Y.F. Lee, M. Schmidt, H. Graalfs, M. Hafner, C. Frech, Modeling of dual gradient elution in ion exchange and mixed-mode chromatography, J. Chromatogr. A 1417 (2015) 64–72, doi:10.1016/j.chroma.2015.09.032.

[39] Y.F. Lee, S. Kluters, M. Hillmann, T. von Hirschheydt, C. Frech, Modeling of bispecific antibody elution in mixed-mode cation-exchange chromatography, J. Sep. Sci. 40 (2017) 3632–3645, doi:10.1002/jssc.201700313.

[40] C. Cobelli, J.J.I. Distefano, Parameter and structural identifiability concepts and ambiguities: a critical review and analysis, Am. Physiol. Soc. (1980) 7–24.

[41] R. Brun, P. Reichert, H.R. Künsch, Practical identifiability analysis of large environmental simulation models, Water Resour. Res. 37 (2001) 1015–1030, doi:10.1029/2000WR900350.
[42] A. Raue, C. Kreutz, T. Maiwald, J. Bachmann, M. Schilling, U. Klingmüller, et al., Structural and practical identifiability analysis of partially observed dynamical models by exploiting the profile likelihood, Bioinformatics 25 (2009) 1923–1929, doi:10.1093/bioinformatics/btp358.
[43] R.N. Gutenkunst, J.J. Waterfall, F.P. Casey, K.S. Brown, C.R. Myers, J.P. Sethna, Universally sloppy parameter sensitivities in systems biology models, PLoS Comput. Biol. 3 (2007) 1871–1878, doi:10.1371/journal.pcbi.0030189.
[44] R.C. Jäpel, J.F. Buyel, Bayesian optimization using multiple directional objective functions allows the rapid inverse fitting of parameters for chromatography simulations, J. Chromatogr. A 1679 (2022), doi:10.1016/j.chroma.2022.463408.
[45] R. Hess, D. Yun, D. Saleh, T. Briskot, J.H. Grosch, G. Wang, et al., Standardized method for mechanistic modeling of multimodal anion exchange chromatography in flow through operation, J. Chromatogr. A 1690 (2023) 463789, doi:10.1016/j.chroma.2023.463789.
[46] T. Hahn, N. Geng, K. Petrushevska-Seebach, M.E. Dolan, M. Scheindel, P. Graf, et al., Mechanistic modeling, simulation, and optimization of mixed-mode chromatography for an antibody polishing step, Biotechnol. Prog. (2022) 1–13, doi:10.1002/btpr.3316.
[47] T. Briskot, T. Hahn, T. Huuk, G. Wang, S. Kluters, J. Studts, et al., Analysis of complex protein elution behavior in preparative ion exchange processes using a colloidal particle adsorption model, J. Chromatogr. A 1654 (2021) 462439, doi:10.1016/j.chroma.2021.462439.
[48] T. Briskot, T. Hahn, T. Huuk, J. Hubbuch, Protein adsorption on ion exchange adsorbers: a comparison of a stoichiometric and non-stoichiometric modeling approach, J. Chromatogr. A 1653 (2021), doi:10.1016/j.chroma.2021.462397.
[49] J.M. Mollerup, A review of the thermodynamics of protein association to ligands, protein adsorption, and adsorption isotherms, Chem. Eng. Technol. 31 (2008) 864–874, doi:10.1002/ceat.200800082.
[50] J.M. Mollerup, T.B. Hansen, S. Kidal, A. Staby, Quality by design-thermodynamic modelling of chromatographic separation of proteins, J. Chromatogr. A 1177 (2008) 200–206, doi:10.1016/J.CHROMA.2007.08.059.
[51] J.M. Mollerup, Applied thermodynamics: a new frontier for biotechnology, Fluid Phase Equilib. 241 (2006) 205–215.
[52] J.M. Mollerup, The thermodynamic principles of ligand binding in chromatography and biology, J. Biotechnol. 132 (2007) 187–195, doi:10.1016/j.jbiotec.2007.05.036.
[53] Schmidt-Traub H. Preparative chromatography: of fine chemicals and pharmaceutical agents. 2005; pp. 216–244 doi:10.1002/3527603484.
[54] Guiochon G., Felinger A., Shirazi D.G., Katti A.M. Fundamentals of preparative chomatography. 2006; pp. 240–257.
[55] T.C. Huuk, T. Hahn, A. Osberghaus, J. Hubbuch, Model-based integrated optimization and evaluation of a multi-step ion exchange chromatography, Sep. Purif. Technol. 136 (2014) 207–222, doi:10.1016/j.seppur.2014.09.012.
[56] T.C. Huuk, T. Briskot, T. Hahn, J. Hubbuch, A versatile noninvasive method for adsorber quantification in batch and column chromatography based on the ionic capacity, Biotechnol. Prog. 32 (2016) 666–677, doi:10.1002/btpr.2228.
[57] A. Staby, S. Ahuja, A.S. Rathore, Model-based preparative chromatography process development in the QbD paradigm, Preparative Chromatography, for Separation of Proteins, Wiley, 2017.
[58] F. Rischawy, D. Saleh, T. Hahn, S. Oelmeier, J. Spitz, S. Kluters, Good modeling practice for industrial chromatography: mechanistic modeling of ion exchange chromatography of a bispecific antibody, Comput. Chem. Eng. 130 (2019), doi:10.1016/j.compchemeng.2019.106532.
[59] D. Saleh, G. Wang, B. Mueller, F. Rischawy, S. Kluters, J. Studts, et al., Cross-scale quality assessment of a mechanistic cation exchange chromatography model, Biotechnol. Prog. 37 (2021), doi:10.1002/btpr.3081.
[60] D. Saleh, G. Wang, F. Rischawy, S. Kluters, J. Studts, J. Hubbuch, In silico process characterization for biopharmaceutical development following the quality by design concept, Biotechnol. Prog. 37 (2021) 1–13, doi:10.1002/btpr.3196.
[61] T.C. Huuk, T. Hahn, K. Doninger, J. Griesbach, S. Hepbildikler, J. Hubbuch, Modeling of complex antibody elution behavior under high protein load densities in ion exchange chromatography using an asymmetric activity coefficient, Biotechnol. J. 12 (2017), doi:10.1002/biot.201600336.
[62] G. Wang, T. Hahn, J. Hubbuch, Water on hydrophobic surfaces: mechanistic modeling of hydrophobic interaction chromatography, J. Chromatogr. A 1465 (2016) 71–78, doi:10.1016/j.chroma.2016.07.085.
[63] V. Kumar, S. Leweke, W. Heymann, E. von Lieres, F. Schlegel, K. Westerberg, et al., Robust mechanistic modeling of protein ion-exchange chromatography, J. Chromatogr. A 1660 (2021), doi:10.1016/j.chroma.2021.462669.
[64] V. Joshi, V. Kumar, A.S. Rathore, Rapid analysis of charge variants of monoclonal antibodies using non-linear salt gradient in cation-exchange high performance liquid chromatography, J. Chromatogr. A 1406 (2015) 175–185, doi:10.1016/J.CHROMA.2015.06.015.
[65] W.K. Son, S.H. Kim, T. Kim Il, Calculation on ion exchange capacity for an ion exchanger using the potentiometric titration, J. Polym. Sci. Part B Polym. Phys. 38 (2000) 3181–3188 AID-POLB180>3.0.CO;2-E, doi:10.1002/1099-0488(20001201)38:23⟨3181.
[66] S. Kumar, S.B. Rai, Spectroscopic studies of L-arginine molecule, Indian J. Pure Appl. Phys. 48 (2010) 251–255.
[67] D.M. Dong, L.Z. Jiao, W.G. Zheng, W.B. Wu, H.K. Feng, C.J. Shen, et al., Determination of nitrite using UV absorption spectra based on multiple linear regression, Asian J. Chem. 25 (2013) 2273–2277, doi:10.14233/ajchem.2013.13840.
[68] M. Zhu, G. Carta, Protein adsorption equilibrium and kinetics in multimodal cation exchange resins, Adsorption 22 (2016) 165–179, doi:10.1007/s10450-015-9735-z.
[69] J.A. Roberts, L. Kimerer, G. Carta, Effects of molecule size and resin structure on protein adsorption on multimodal anion exchange chromatography media, J. Chromatogr. A 1628 (2020) 461444, doi:10.1016/j.chroma.2020.461444.
[70] M.J. Armstrong, A.N. Beris, N.J. Wagner, An adaptive parallel tempering method for the dynamic data-driven parameter estimation of nonlinear models, AIChE J. 63 (2017) 1937–1958, doi:10.1002/aic.15577.
[71] S.O. Rastegar, T. Gu, Empirical correlations for axial dispersion coefficient and Peclet number in fixed-bed columns, J. Chromatogr. A 1490 (2017) 133–137, doi:10.1016/j.chroma.2017.02.026.
[72] E.J. Wilson, C.J. Geankoplis, Liquid mass transfer at very low reynolds numbers in packed beds, Ind. Eng. Chem. Fundam. 5 (1966) 9–14, doi:10.1021/i160017a002.
[73] G. Carta, A. Jungbauer, in: Protein Chromatography: Process Development and Scale-Up, John Wiley & Sons, Ltd, 2020, pp. 165–170.
[74] C.N. Satterfield, Mass Transfer in Heterogeneous Catalysis, MIT Press, 1970.
[75] H. Brenner, L.J. Gaydos, The constrained brownian movement of spherical particles in cylindrical pores of comparable radius. Models of the diffusive and convective transport of solute molecules in membranes and porous media, J. Colloid Interface Sci. 58 (1977) 312–356, doi:10.1016/0021-9797(77)90147-3.
[76] J.L. Anderson, J.A. Quinn, Restricted transport in small pores: a model for steric exclusion and hindered particle motion, Biophys. J. 14 (1974) 130–150, doi:10.1016/S0006-3495(74)70005-4.
[77] W.K. Hartmann, N. Saptharishi, X.Y. Yang, G. Mitra, G. Soman, Characterization and analysis of thermal denaturation of antibodies by size exclusion high-performance liquid chromatography with quadruple detection, Anal. Biochem. 325 (2004) 227–239, doi:10.1016/j.ab.2003.10.031.
[78] A.M. Lenhoff, Multiscale modeling of protein uptake patterns in chromatographic particles, Langmuir 24 (2008) 5991–5995, doi:10.1021/la8004163.
[79] T. Hahn, T. Huuk, V. Heuveline, J. Hubbuch, Simulating and optimizing preparative protein chromatography with ChromX, J. Chem. Educ. 92 (2015) 1497–1502, doi:10.1021/ed500854a.
[80] W. Heymann, J. Glaser, F. Schlegel, W. Johnson, P. Rolandi, E. von Lieres, Advanced score system and automated search strategies for parameter estimation in mechanistic chromatography modeling, J. Chromatogr. A 1661 (2022) 462693, doi:10.1016/j.chroma.2021.462693.
[81] K.P. Burnham, D.R. Anderson, Multimodel inference: understanding AIC and BIC in model selection, Sociol. Methods Res. 33 (2004) 261–304, doi:10.1177/0049124104268644.
[82] E.J. Wagenmakers, S. Farrell, AIC model selection using Akaike weights, Psychon. Bull. Rev. 11 (2004) 192–196, doi:10.3758/BF03206482.
[83] J.E. Cavanaugh, A.A. Neath, The Akaike information criterion: background, derivation, properties, application, interpretation, and refinements, Wiley Interdiscip. Rev. Comput. Stat. 11 (2019) 1–11, doi:10.1002/wics.1460.
[84] M.D. Morris, Factorial sampling plans for preliminary computational experiments, Technometrics 33 (1991) 161–174.
[85] I.M. Sobol, Global sensitivity indices for nonlinear mathematical models and their Monte Carlo estimates, Math. Comput. Simul. 55 (2001) 271–280, doi:10.1016/S0378-4754(00)00270-6.
[86] B.D. Kelley, S.A. Tobler, P. Brown, J.L. Coffman, R. Godavarti, T. Iskra, et al., Weak partitioning chromatography for anion exchange purification of monoclonal antibodies, Biotechnol. Bioeng. 101 (2008) 553–566, doi:10.1002/bit.21923.